Supplement of Earth Syst. Sci. Data, 17, 1873–1958, 2025
https://doi.org/10.5194/essd-17-1873-2025-supplement

Open Access Earth System Science Data

Supplement of

Global Methane Budget 2000–2020

Marielle Saunois et al.

Correspondence to: Marielle Saunois (marielle.saunois@lsce.ipsl.fr)

Contents

List of Tables

List of Figures

S1 Contents of the main manuscript

Here we provide the Contents list of the main manuscript.

S2 Comparisons with AR5 and AR6 projections

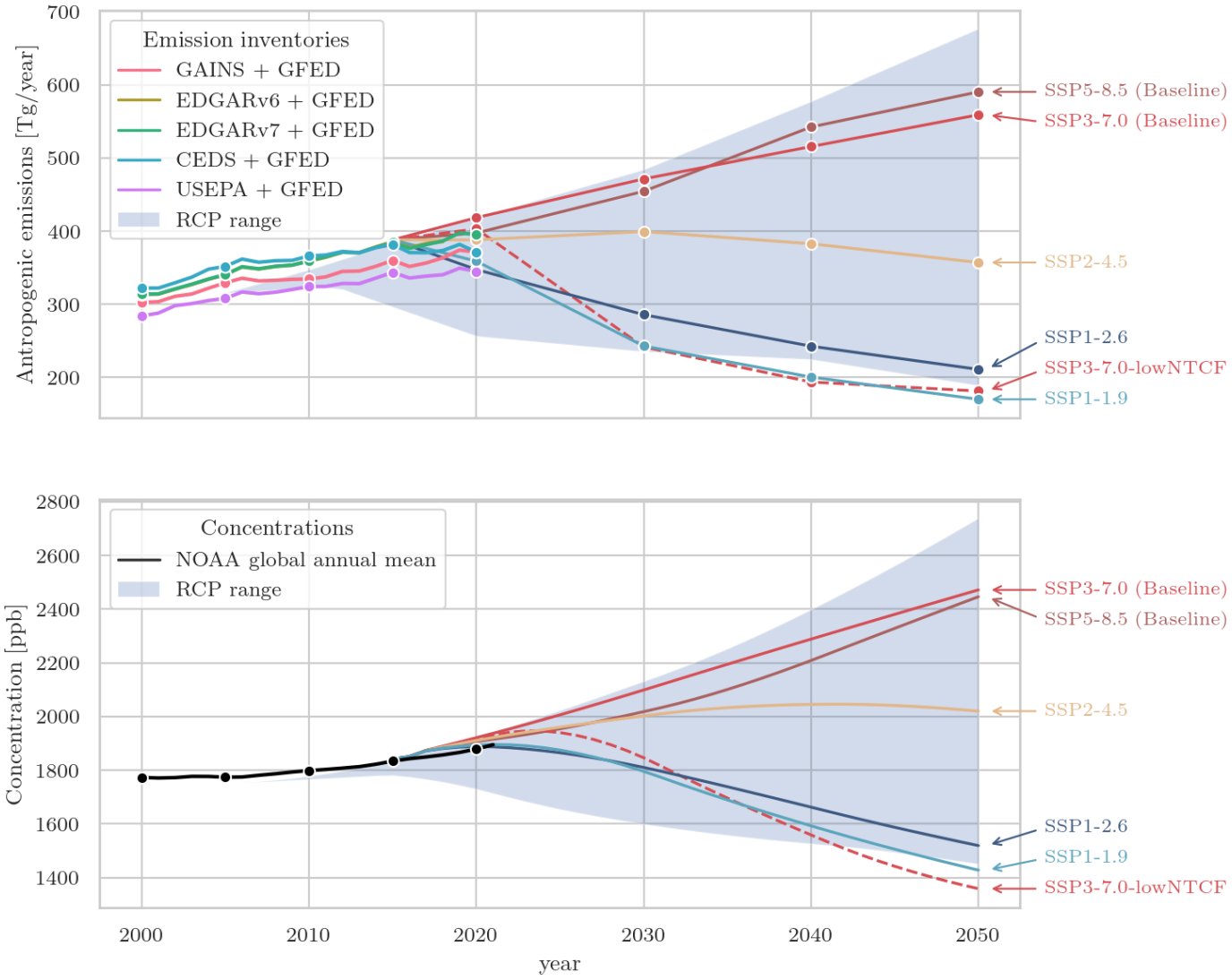

Figure S1: Time series of methane anthropogenic emissions (top) and atmospheric concentrations (bottom). RCPs (from AR5) and SSPs (from AR6) are shown on top of the anthropogenic total emission estimates from this study for emissions (top) and NOAA global mean atmospheric concentrations (bottom).

S3 Supplementary text 1: Principle of inversions

An atmospheric inversion for methane fluxes (sources and sinks) optimally combines atmospheric observations of methane and associated uncertainties, a prior knowledge of the fluxes including their uncertainties, and a chemistry-transport model to relate fluxes to concentrations (Rodgers, 2000). In this sense, top-down inversions integrate all the components

of the methane cycle described previously in this paper. The observations can be surface or upper-air in situ observations, satellite and surface retrievals. Prior emissions generally come from bottom-up approaches such as process-based models or data-driven extrapolations (natural sources) and inventories (anthropogenic sources). The chemistry-transport model can be Eulerian or Lagrangian, and global or regional, depending on the scale of the flux to be optimized. Atmospheric inversions generally rely on the Bayes theorem, which leads to the minimization of a cost function as Eq.S1:

$$J(x) = \frac{1}{2}(y - H(x))^T R^{-1}(y - H(x)) + \frac{1}{2}(x - x_b)^T B^{-1}(x - x_b) \tag{S1}$$

where y is a vector containing the atmospheric observations, x is a state vector containing the methane emissions and other appropriate variables (like OH concentrations or CH_4 concentrations at the start of the assimilation window) to be estimated, x_b is the prior state of x, and H is the observation operator, here the combination of an atmospheric transport and chemistry model and an interpolation procedure sampling the model at the measurement coordinates. R is the error covariance matrix of the observations and P_b is the error covariance matrix associated to. The errors on the modelling of atmospheric transport and chemistry are included in the R matrix (Tarantola, 1987). The minimization of a linearized version of J leads to the optimized state vector x_a (Eq.S2):

$$x_a = x_b + (H^T R^{-1} H + P_b^{-1})^{-1} H^T R^{-1}(y - H(x)) \tag{S2}$$

where P_a is given by Eq.S3 and represents the error covariance matrix associated to x_a, and H contains the sensitivities of any observation to any component of state vector x (linearized version of the observation operator H(x)).

$$P_a = (H^T R^{-1} H + P_b^{-1})^{-1} \tag{S3}$$

Unfortunately, the size of the inverse problem usually does not allow computing P_a, which is therefore approximated using the leading eigenvectors of the Hessian of J (Chevallier et al., 2005) or from stochastic ensembles (Chevallier et al., 2007). Therefore, the optimized fluxes x_a are obtained using classical minimization algorithms (Chevallier et al., 2005; Meirink et al., 2008b). Alternatively, Chen and Prinn (2006) computed monthly emissions by applying a recursive Kalman filter in which P_a is computed explicitly for each month. Emissions are generally derived at weekly to monthly time scales, and for spatial resolutions ranging from model grid resolution to large aggregated regions. Spatio-temporal aggregation of state vector elements reduces the size of the inverse problem and allows the computation of P_a. However, such aggregation can also generate aggregation errors inducing possible biases in the inferred emissions and sinks (Kaminski et al., 2001). The estimated x_a can represent either the net methane flux in a given region or contributions from specific source categories. Atmospheric inversions use bottom-up models and inventories as prior estimates of the emissions and sinks in their setup, which make B-U and T-D approaches generally not independent.

S4 Supplementary text 2: Set of prior fluxes proposed by the atmospheric inversion protocol

A set of fluxes for the different methane sources has been gathered and made available to the community to perform atmospheric inversions.
We have used :

- biomass burning from GFED4.1s on a monthly basis up to 2020.
- the dynamical (monthly) wetlands emissions from the ensemble mean of 11 models contributing to the Global Methane Budget (Saunois et al. 2020)
- termite emissions from the model described in Saunois et al. (2020), representing a climatological estimate.
- emissions from oceans from Weber et al. (2019) geological emissions from Etiope et al. (2019) scaled to 23 Tg for global emission based on IPCC AR6 best estimates. This estimate is higher than Hmiel et al.(2020), but lower than Etiope et al., (2019). Offshore and onshore estimates were provided. We suggested to use only land emissions (onshore) to avoid double-counting offshore geological emissions with these from the "ocean" emission.
- the soils uptake is Saunois et al. (2020), based on Murgia-Flores et al. (2018).

We performed two rounds of inversions (v1 and v2).
The first round of inversions uses anthropogenic emissions from EDGARv6 database (Crippa et al., 2021; Oreggioni et al., 2021; EDGARv6 website `https://edgar.jrc.ec.europa.eu/dataset_ghg60`; Ferrario et al., 2021), which is available up to 2018.

For this study, the EDGARv6 was extrapolated up to 2019 using the FAO-CH4 emissions for CH_4 emissions from enteric fermentation, manure management and rice cultivation, and using the BP statistical review of fossil fuel production and consumption (http://www.bp.com/) to update CH_4 emissions from coal, oil and gas sectors. 2020 and 2021 emissions were set equal 2019 emissions.

Later, it was further extended to 2020 for the main budget. In this extrapolated inventory, called EDGARv6EXT, methane emissions for year t are set up equal to the 2018 EDGAR CH_4 emissions (E_EDGARv6) times the ratio between the FAO-CH4 emissions (or BP statistics) of year t (E_FAO-CH4(t)) and FAO-CH4 emissions (or BP statistics) of 2018 (E_FAO-CH4(2018)). For each emission sector, the region-specific emissions (E_EDGARv6ext) in year (t) are estimated following Eq.S4:

$$E_{EDGARv6}(t) = E_{EDGARv6}(2018) * E_{FAO-CH4}(t)/E_{FAO-CH4}(2018) \quad \text{(S4)}$$

Transport, industrial, waste and biofuel sources were linearly extrapolated based on the last three years of data while other sources are kept constant at the 2018 level. This extrapolation approach is necessary, and often performed by top-down approaches to define prior emissions, because, up to now, global inventories such as sector-specific emissions in the EDGAR database are not updated on a regular basis.

A second round of inversion was performed by most of the groups using the GAINS gridded data set instead of EDGARv6 for all the fossil fuel related emissions. This was done due to a significant change on boreal emissions in EDGARv6 probably related to changes in data activity maps.

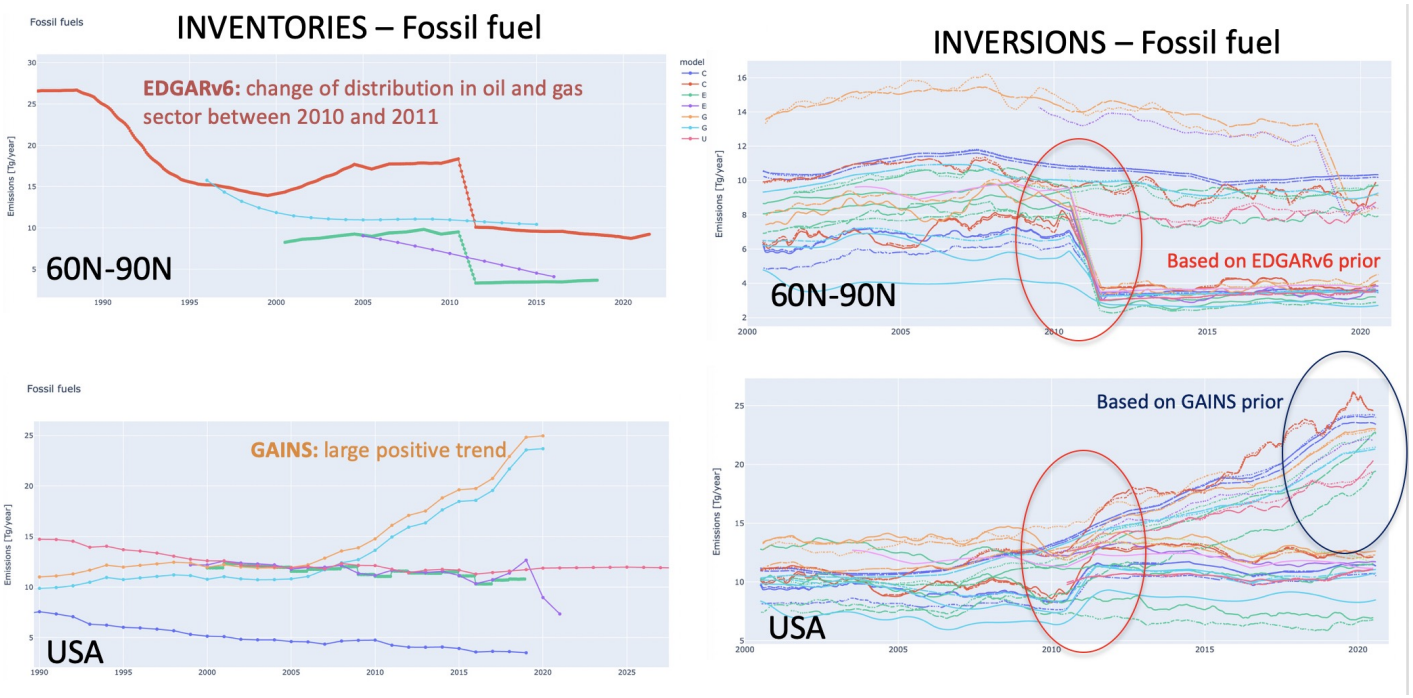

Figure S2: Emission in the fossil fuel sector in the inventories (left) and after data assimilation in inversions (right) for the boreal region (top) and the USA (bottom).

S5 Definition of the regions

Figure S3: Map of the 18 continental regions.

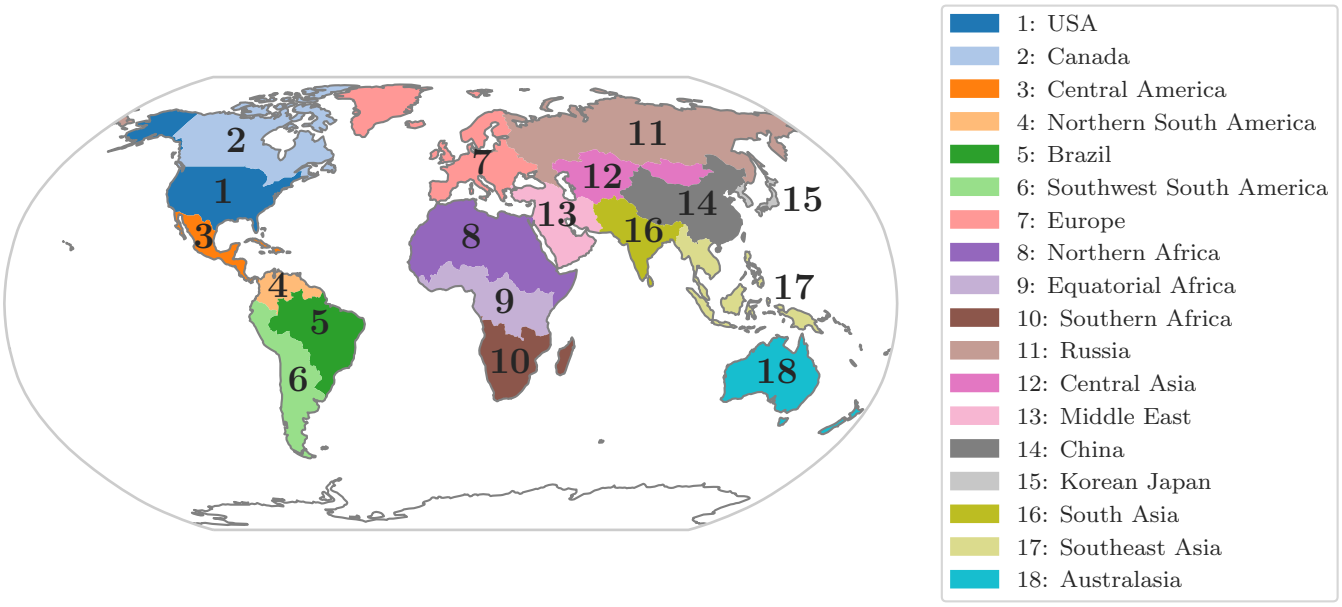

Table S1: List of the countries used to define the 18 continental regions. Compared to Saunois et al. (2020), regions are the same except for the last region includes only Australia and New-Zealand and is called *Australasia*.

N°	**Region name**	**Countries or territories**
1	USA	USA with Alaska, Bermuda Islands
2	Canada	Canada
3	Central America	Anguilla, Antigua and Barbuda, Bahamas, Barbados, Belize, British Virgin Islands, Cayman Islands, Costa Rica, Cuba, Dominica, Dominican Republic, El Salvador, Guadeloupe, Guatemala, Honduras, Jamaica, Martinique, Mexico, Montserrat, Nicaragua, Panama, Puerto Rico, Saint Kitts and Nevis, Saint Lucia, Saint Vincent and the Grenadines, Turks and Caicos Islands, United States Virgin Islands
4	Brazil	Brazil
5	Northern South America	Aruba, Colombia, French Guiana, Grenada, Guyana, Suriname, Trinidad and Tobago, Venezuela
6	Southwest South America	Argentina, Bolivia, Chile, Ecuador, Peru, Falkland Islands (Malvinas), Paraguay, Uruguay
7	Europe	Albania, Andorra, Austria, Belarus, Belgium, Belgium, Luxembourg, Bulgaria, Channel Islands, Croatia, Cyprus, Czech Republic, Denmark, Estonia, Faroe Islands, Finland, France, Germany, Gibraltar, Greece, Greenland, Hungary, Iceland, Ireland, Isle of Man, Italy, Latvia, Liechtenstein, Lithuania, Luxembourg, Malta, Montenegro, Netherlands, Norway, Poland, Portugal, Republic of Moldova, Romania, Serbia, Slovakia, Slovenia, Spain, Sweden, United Kingdom, Ukraine
8	Northern Africa	Algeria, Cabo Verde, Chad, Côte d'Ivoire, Djibouti, Egypt, Eritrea, Ethiopia, Ethiopia PDR, Gambia, Guinea, Guinea-Bissau, Libya, Mali, Mauritania, Morocco, Saint Helena Ascension and Tristan da Cunha, Sao Tome and Principe, Senegal, Somalia, Sudan former, Tunisia, Western Sahara
9	Equatorial Africa	Benin, Burkina Faso, Burundi, Cameroon, Central African Republic, Congo, Democratic Republic of the Congo, Equatorial Guinea, Gabon, Ghana, Liberia, Nigeria, Rwanda, Sierra Leone, Togo, Uganda, United Republic of Tanzania
10	Southern Africa	Angola, Botswana, Comoros, Lesotho, Madagascar, Malawi, Mauritius, Mayotte, Mozambique, Namibia, Reunion, Seychelles, South Africa, Swaziland, Zambia, Zimbabwe
11	Russia	Russian federation
12	Central Asia	Kazakhstan, Kyrgyzstan, Tajikistan, Turkmenistan, Uzbekistan, Mongolia
13	Middle East	Armenia, Azerbaijan, Bahrain, People's Republic of Georgia, Iran, Iraq, Israel, Jordan, Kuwait, Lebanon, Occupied Palestinian Territory, Oman, Qatar, Saudi Arabia, Syrian Arab Republic, Turkey, United Arab Emirates, Yemen
14	China	China mainland, Macao, Hong Kong, Taiwan
15	Korea and Japan	Japan, Korea, Republic of Korea
16	South Asia	Afghanistan, Bangladesh, Bhutan, India, Nepal, Pakistan, Sri Lanka
17	South East Asia	American Samoa, Brunei Darussalam, Cambodia, Cook Islands, Fiji, French Polynesia, Guam, Indonesia, Kiribati, Lao People's Democratic Republic, Malaysia, Maldives, Marshall Islands, Myanmar, Nauru, New Caledonia, Niue, Norfolk Island, Northern Mariana Islands, Pacific Islands Trust Territory, Palau, Papua New Guinea, Pitcairn Islands, Philippines, Samoa, Singapore, Solomon Islands, Thailand, Timor-Leste, Tokelau, Tonga, Tuvalu, Vanuatu, Vietnam, Wallis and Futuna Islands
18	Australasia	Australia, New Zealand

S6 Tables and figures supporting the bottom-up-budget section

Table S2: Assignment of the inventory specific sectors to GCP sub and main categories

	Category	EDGARv6.0	GAINS by country	GAINS gridded	CEDS	USEPA
Agriculture and Waste	Enteric fermentation and Manure	ENF (Enteric fermentation) MNM (Manure management)	Beef_cattle Dairy_cows Pigs Other_livestock	agr_cow (cattle) agr_buff (buffaloes) agr_pig (pigs) agr_gosh (sheep and goats) agr_poult (poultry) agr (other)	Agriculture (incl. Rice)	Livestock
	Rice cultivation	AGS (Agricultural soils)	Rice_cultivation	agr_fert (soils)		Rice OtherAg
	Landfills and Waste	SWD_LDF (Solid waste landfills) SWD_INC (Solid waste incineration) WWT (Waste water handling)	Solid_waste_industry Solid_waste_municipal Wastewater_industry Wastewater_domestic	wst wst_rur wst_urb	Waste	Landfills Wastewater OtherWaste
Fossil Fuels	Oil & Gas	PRO_OIL (Fuel exploitation OIL) PRO_GAS (Fuel exploitation GAS) FFF (Fossil Fuel Fires)	Oil_production Oil_refinery Gas_production Gas_distribution Unconventional_gas_prod	flr_up (Oil and gas production)	Energy (incl. Coal)	NGO
	Coal	PRO_COAL (Fuel exploitation COAL)	Coal_mining Abandoned_coal_mines	mbc (Coal mining) mhc (Coal mining)		Coal
	Industry	CHE (Chemical processes) IRO (Iron and steel production) ENE (Power industry) IND (Combustion for manufacturing) REF_TRF (Oil refineries and– –Transformation industry)	Gas_transmission	ind (Industry) pp_bio (Power plants -biofuel) pp_coal (Power plants -coal) pp_eng (Power engines) pp_gas (Power plants -gas) pp_oil (Power plants -oil)	Industrial Solvents production– –and application	OtherEnergy OtherIPPU
	Transport	TRO_noRES (Road transportation no resuspension) TNR_Aviation_CDS (Aviation climbing & descent) TNR_Aviation_CRS (Aviation cruise) TNR_Aviation_LTO (Aviation landing & takeoff) TNR_Aviation_SPS (Aviation supersonic) TNR_Other (Railways, pipelines, off-road transport) TNR_Ship (Shipping)	Combustion_fossil_fuel	tra_rd_2w (2 wheelers) tra_rd_hdb (Buses) tra_rd_hdt (Trucks) tra_rd_ld4 (Cars)	Transportation International Shipping	Combustion (StatMob)
	Biofuels burning	RCO (Energy for buildings)	Combustion_biomass_fuel	dom_cook_r (Rural households) dom_cook_u (Urban households) dom_heat_r (Rural households)	Residential, Com– –mercial, Other	Combustion (Biomass)

Table S3: Contributions of the land surface models to compute methane wetland emissions to the different releases of the global methane budget.

Model name	Kirschke et al. (2013)	Saunois et al. (2016) Poulter et al. (2017)	Saunois et al. (2020)	This study
CH4MOD	–	–	–	Y
CLASS-CTEM // CLASSIC	–	Y	Y	Y
CLM4.5	–	Y	–	–
DLEM	–	Y	Y	Y
ELM-ECA	–	–	Y	Y
ISAM	–	–	–	Y
JSBACH	–	–	Y	Y
JULES	–	Y	Y	Y
LPJ-GUESS	–	–	Y	Y
LPJ-MPI	–	Y	Y	Y
LPJ-wsl	Y	Y	Y	Y
LPX-Bern	Y	Y	Y	Y
ORCHIDEE	Y	Y	Y	Y
SDGVM	–	Y	–	Y
TEM-MDM	–	–	Y	Y
TRIPLEX-GHG	–	Y	Y	Y
VISIT	–	Y	Y	Y
Contributing	3	11	13	16

Table S4: Tropospheric OH concentrations in 10^6 molec cm^{-3} and inter annual variability (IAV) in % from the ensemble of model contributing to CCMI-2022 (Plummer et al., 2021) and CMIP6 (Collins et al., 2017) modeling activities. Values are given as average values over the period 2000-2010 for CCMI-2022 and CMIP6 and for 2010-2018 for CCCMI-2022 only.

	mean [mil. molec/cm^3]	IAV [%]
CCMI-2022 - 2000-2010		
ACCESS-CM2-Chem	1.22	1.2
CCSRNIES-MIROC32[b]	2.37	2.4
CMAM	1.29	1.3
CNRM-MOCAGE	1.34	1.3
EMAC-CCMI2	1.23	1.2
GEOSCCM	1.20	1.2
IPSL-CM6A-ATM-LR-REPROBUS[a]	0.17	0.2
NIWA-UKCA2	1.17	1.2
SOCOL	1.82	1.8
UKESM1-StratTrop	1.39	1.4
mean of 8 models [min-max]	1.33 [1.17 - 1.82]	
CMIP6 - 2000-2010 - Historical run		
BCC-ESM1 [b]	0.79	0.8
CESM2-FV2	1.20	1.2
CESM2-WACCM-FV2	1.35	1.3
CESM2-WACCM	1.20	1.2
CESM2	1.20	1.2
CNRM-ESM2-1 [b]	0.47	0.5
EC-Earth3-AerChem	1.20	1.2
GISS-E2-1-G	1.34	1.3
GISS-E2-2-G	1.26	1.3
MPI-ESM-1-2-HAM	0.97	1.0
MRI-ESM2-0	0.94	0.9
mean of 10 models [min-max]	1.15 [0.79-1.35]	
CCMI-2022 - 2010-2018		
ACCESS-CM2-Chem	1.22	1.2
CCSRNIES-MIROC32[b]	2.38	2.4
CMAM	1.30	1.3
CNRM-MOCAGE	1.27	1.3
EMAC-CCMI2	1.25	1.2
GEOSCCM	1.21	1.2
IPSL-CM6A-ATM-LR-REPROBUS[a]	0.17	0.2
NIWA-UKCA2	1.17	1.2
SOCOL	1.85	1.9
UKESM1-StratTrop	1.40	1.4
mean [min-max] of 8 models	1.33 [1.17-1.85]	

[a] no tropospheric chemical scheme in this model - removed from the ensemble
[b] outlier - removed from the ensemble

Table S5: Methane chemical loss in the troposphere[a] and stratosphere in Tg yr^{-1} on average the decade 2000-2009 and 2010-2019 as calculated by chemistry climate models contributing to CMIP6 (Collins et al., 2017) modeling activities. Values are provided for both the historical run (Hist- SSP3-7.0 starting in 2015), and the AMIP experiments. The AMIP experiments use prescribed SSTs and Sea Ice rather than a coupled ocean.

	Tropospheric loss	Stratospheric loss	Total chemical loss	Tropospheric lifetime[b]	Total lifetime[c]
CMIP6 (2000-2009) - Historical run + SSP3-7.0 Starting in 2015					
BCC-ESM1[d]	794.3	27.2	821.5	6.2	5.7
CESM2-WACCM	663.3	39.9	703.2	7.5	6.8
EC-Earth3-AerChem	557.2	10.2[e]	567.4	8.8	8.2
GISS-E2-1-G	527.7	51.2	578.9	9.3	8.1
GISS-E2-1-H	510.4	41.2	551.6	9.7	8.5
MRI-ESM2-0	446.5	33.3	479.8	11.0	9.7
mean [min-max]	541 [446-663]	39 [27-51]	576 [480-703]	9.3 [7.5-11.0]	8.2 [6.8-9.7]
CMIP6 - AMIP experiment (2000-2009)					
BCC-ESM1[d]	799.1	27.4	826.5	6.1	5.7
CESM2-WACCM-FV2	606.8	38.1	644.9	8.1	7.3
CESM2-WACCM	650.9	39.3	690.2	7.6	6.9
EC-Earth3-AerChem	552.7	10.2[e]	562.9	8.9	8.3
GISS-E2-1-G	487.6	41.2	528.8	10.1	8.8
MRI-ESM2-0	452.3	32.8	485.1	10.9	9.5
mean [min-max]	550 [452-650]	36 [27-41]	582 [485-690]	9.1 [7.7-10.9]	8.2 [6.9-9.5]
Ensemble of 10 runs - Historical and AMIP runs (2000-2009)					
mean [min-max]	546 [446-663]	37 [27-51]	579 [480-703]	9.2 [7.5-11.0]	8.2 [6.8-9.7]
CMIP6 (2010-2019) - Historical run + SSP3-7.0 Starting in 2015					
BCC-ESM1[d]	836.6	27.8	864.4	6.0	5.6
CESM2-WACCM	693.4	40.9	734.3	7.4	6.7
EC-Earth3-AerChem	582.2	10.7[e]	592.9	8.7	8.1
GISS-E2-1-G	540.8	43.3	584.1	9.4	8.3
GISS-E2-1-H	537.0	37.6	574.7	9.5	8.5
MRI-ESM2-0	462.3	33.4	495.7	11.0	9.7
mean [min-max]	563 [462-663]	37 [28-43]	596 [496-734]	9.2 [7.4-11.0]	8.2 [6.7-9.7]

[a] tropopause height at 200hPa
[b] defined as total burden divided by tropospheric loss
[c] defined as total burden divided by total loss. Total loss = total chemical loss (tropospheric and stratospheric losses) + 31 Tg from soil uptake for consistency with the main text budget. Note that changing the amount of soil uptake to 35 Tg will not change the results significantly (about 0.1 year).
[d] outlier regarding the tropospheric loss - removed from the calculation
[e] outlier regarding the stratospheric loss - removed from the calculation

Table S6: Soil uptake estimates from the literature and in the Global Methane Budget in Tg CH_4 yr^{-1}

Reference	Method	Period	Best estimate	Range	Range explanation
Ridgwell et al. (1999)	Modelling	1990s	38	20-51	Model struct. uncertainty
Dutaur and Verchot (2007)	Extrapolation of obs.	?	22	10-34	
Curry (2007)	Modelling- CLASS	1979–1999	28	9-47	
Riley et al. (2011)	Modeling - CLM4Me	?	31	15-38	Struc. uncertainties
Ito and Inatomi (2012)	Modelling - VISIT	1996-2005		25-35	
Tian et al. (2016)	Modelling - DLEM	2000-2009	30	11-49	
Murguia-Flores et al. (2018)	Modelling – MeMo	2008-2017[a]	32	29-38	Different parametrizations
	Modelling – MeMo	2000-2009[b]	35	30-38	Different parametrizations
	Modelling – MeMo	2010-2019[b]	36	31-39	Different parametrizations
Kaiser et al. (2017)	Modelling – JSBACH	2000-2009[b]	17		
Kaiser et al. (2017)	Modelling – JSBACH	2010-2019[b]	18		
Ito and Inatomi et al. (2012)	Modelling – VISIT	2000-2009[b]	34		
Ito and Inatomi et al. (2012)	Modelling – VISIT	2010-2019[b]	37		
Synthesis publications	**Litterature based on**		**Mean**	**Range**	
Kirschke et al. (2013)	Curry (2007)		28	9-47	
Saunois et al. (2016)	Curry (2007)		28	9-47	
Saunois et al. (2020)	Tian et al. (2016)	2000-2009	30	11- 49	
This study		2000-2009	31	17-39	
This study		2010-2019	32	18-40	

[a] runs have been performed specifically for this period for Saunois et al. (2020)
[b] runs have been performed specifically for this period for this study

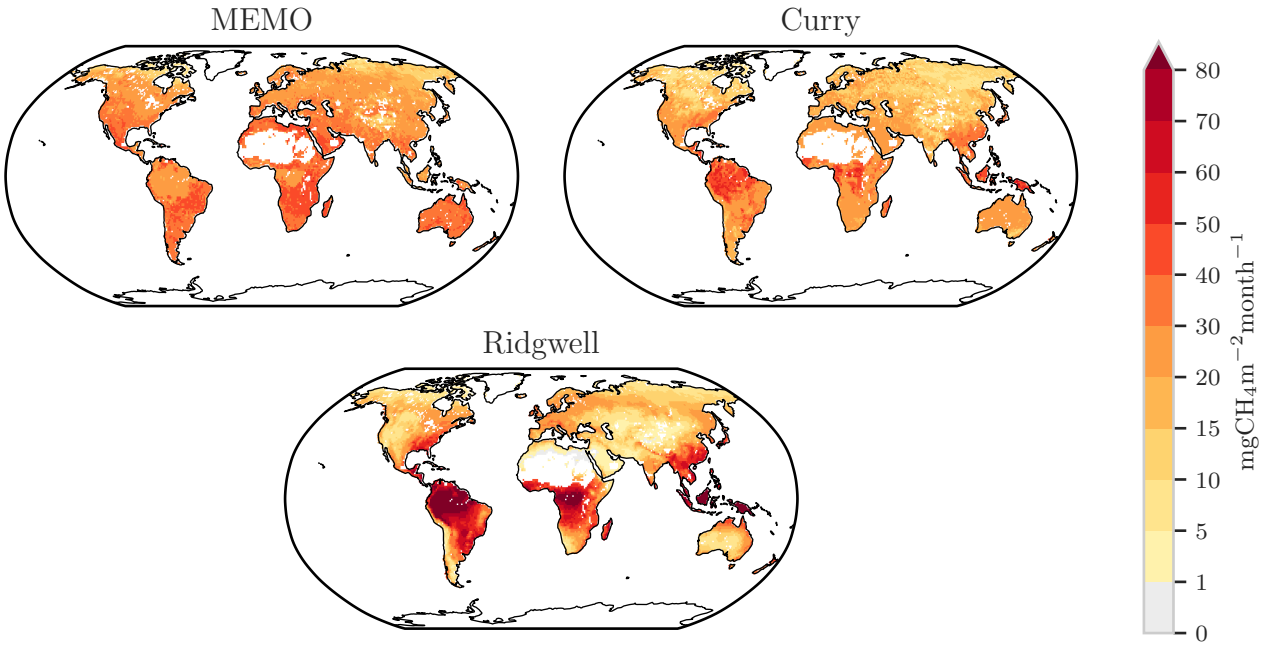

Figure S4: Distribution of the soil uptake from three different studies : MeMo (Murgia-Flores et al., 2018), Curry et al. (2007) and Ridgewell et al. (1999).

S7 Table supporting the top-down budget section

Table S7: Contributions of the different inverse systems to the different releases of the global methane budget.

Model name	Kirschke et al. (2013)	Saunois et al. (2016)	Saunois et al. (2020)	This study
CTE-CH4 (NOAA)	Surface	Surface	–	–
CTE-CH4 (FMI)	–	–	Surface/GOSAT	Surface
GELCA	–	Surface	Surface	–
GEOSCHEM	Surface	–	–	–
GISS	Surface	–	–	–
LMDz-CIF	–	–	–	Surface
LMDz-MIOP	Surface	Surface	–	–
LMDz-PYVAR	Surface	Surface/GOSAT	Surface/GOSAT	GOSAT
MATCH	Surface	–	–	–
MIROC4-ACTM	–	Surface	Surface	Surface
NICAM-TM	–	–	Surface	Surface
NIESTM	–	Surface/GOSAT	Surface/GOSAT	Surface/GOSAT
TM2	Surface	–	–	–
TM5-CAMS (TM5-SRON)	Surface	Surface/GOSAT	Surface/GOSAT	Surface/GOSAT
TM5-JRC	Surface	Surface/GOSAT	Surface/GOSAT	–
TOMCAT	–	–	Surface	–
Contributing	9	8	9	7

Table S8: Characteristics of the top-down inverse systems contributing to this study. CTE-CH4, LMDz- CIF, abd LMDz-PYVAR. 1/2

		CTE-CH4	LMDz- CIF	LMDz-PYVAR
Main ref.		Tsuruta et al. (2017)	Thanwerdas et al. (2022)	Zheng et al. (2018a, 2018b)
Model Characteristics	Meteorology	ECMWF ERA5	LMDz nudged to ERA-I	LMDz nudged to ERA5
	Resolution	Global 6x4 + two-way nested 1x1 zoom over Europe, 25 levels	(3.75° longitude × 1.9° latitude × 39 layers)	(3.75° longitude × 1.9° latitude × 39 layers)
	PBL scheme	Based on parameterisation of Vogelezang and Holtslag (1996) (Krol et al., 2018)	ECMWF ERA-Interim 6 hourly PBL height	ECMWF ERA5 6 hourly PBL height
	Convection Scheme	Gregory et al., 2000	Tiedtke's scheme	Tiedtke's scheme
Inversion set-up	Time resolution	1 week	8 days	8 days
	Spatial resolution	1x1 over Europe, Russia, USA and Canada. Region-wise elsewhere	3.75° longitude × 1.9° latitude	3.75° longitude × 1.9° latitude
	Prior errors	80% of flux over land, 20% over ocean	70% of prior emissions	70% of prior emissions
	Correlation length	100 km over 1x1 region, 500 km over other land regions, 900 km over ocean	1000 km (ocean), 500 km (land), 16 days (temporal)	1000 km (ocean), 500 km (land), 16 days (temporal)
	Minimizers	Ensemble Kalman filter (Peters et al., 2005)	M1QN3	M1QN3
	Control vector (temporal and sectorial resolution)	1 week, 2 categories: anthropogenic + biomass burning + rice, wetlands + soil uptake	10 days, 12 emission fluxes categories, 3.75° longitude × 1.9° latitude	8 days, total emission fluxes, 3.75° longitude × 1.9° latitude
Prior sources	Anthropogenic	GCP	GCP	GCP
	Biomass burning	GCP	GCP	GCP
	Wetlands	GCP	GCP	GCP
	Rice	GCP	GCP	GCP

Table S9: Characteristics of the top-down inverse systems contributing to this study. CTE-CH4, LMDz- CIF, abd LMDz-PYVAR. 2/2

		CTE-CH4	LMDz- CIF	LMDz-PYVAR
Prior Sources	Termites	GCP	GCP	GCP
	Other	GCP (geological and oceans)	GCP (geological and oceans)	GCP (geological and oceans)
Prior sinks	Soil uptake	GCP	GCP	GCP
	Chemistry	OH, O1D, Cl Transcom-CH4 (Patra et al., 2011)	OH, O1D Transcom-CH4 (Patra et al., 2011)	OH, O1D Transcom-CH4 (Patra et al., 2011)
Assimilated Data	Surface Obs.	AGAGE, CSIRO, EC, FMI, LSCE, NIES, NOAA, (part of) WDCGG, MPI-BGC, University of Exeter	AGAGE, CSIRO, EC, FMI, LSCE, NIES, NOAA, (part of) WDCGG, MPI-BGC, University of Exeter	
	Satellite data		-	GOSAT University of Leicester v9.0
	Satellite data processing if any		-	
Observation errors	Surface observation	4.5 to 75 ppb, depending on sites. No spatial/temporal correlation.	4.5 to 75 ppb, depending on sites. No spatial/temporal correlation.	-
	Satellite Data		-	Grid dependent. 150-200 ppb that includes instrument, representation, and forward model errors.
Time window		1 week	June 1999- June 2021	24 months each year (Jul-Jun)
Time period covered		2000-2020	Surface : 2000-2020	Satellite: 2010-2020

Table S10: Characteristics of the top-down inverse systems contributing to this study. MIROC4-ACTM, NIESMON-CH4, NIES-TM-FLEXPART, and TM5-CAMS. 1/2

		MIROC4-ACTM	NIESMON-CH4	NIES-TM-FLEXPART	TM5-CAMS
Main ref.		Patra et al. (2018); Watanabe et al. (2008)	Niwa et al. (2022; 2024)	Maksyutov et al. (2021); Wang (2019a)	Segers et al. (2022, report); Bergamaschi et al. (2010; 2013), Panday et al. (2016)
Model Characteristics	Meteorology	JRA-55 (Kobayashi et al., 2015)	JRA-55 (Kobayashi et al., 2015; Harada et al., 2016)	JCDAS/JRA-55 (FLEXPART), ERA5 (NIES-TM)	ECMWF ERA-Interim, forecasts 3-12 hour, 3 hourly temporal resolution
	Resolution	2.8 x 2.8 x 67	223 km, 40 levels (model top 45km)	3.75° × 3.75° × 42 levels NIES-TM, 0.1° × 0.1° FLEXPART	3 x 2 x 34
	PBL scheme	Mellor and Yamada (1974, 1982)	Mellor and Yamada (1974) & Nakanishi and Niino (2004)	ERA5 turbulent diffusion	LTG (Louis, Tiedtke and Geleyn) following Holtslag and Boville (1993)
	Convection Scheme	Arakawa and Schubert (1974)	Chikira and Sugiyama (2010)	ERA5 convective mass fluxes	ERA-Interim archived convective fluxes
Inversion set-up	Time resolution	Monthly	monthly	15 days	Monthly
	Spatial resolution	2.8 x 2.8	1° × 1°	0.1° × 0.1°	3 x 2 x 34
	Prior errors	50% of the fluxes over all the basis regions	calculated from the ensemble of VISIT for wetlands, rice cultivation, and soil uptake, and set 30 % for the others	EDGAR 6.0 for anthropogenic (30% of prior, each category), and GCP wetlands (50% of prior) emissions	100% for categories wetlands, rice, and biomass burning; 50% for category with remaining sources (mainly anthropogenic)
	Correlation length	0 between all the basis regions	calculated from the ensemble of VISIT for wetlands, rice cultivation, and soil uptake, and set 0 km for coal, oil &gas, biomass burnings, and set 500 km for the others	500 km (spatial), 15 days (temporal)	500 km
	Minimizers	Bayesian method	POpULar (Fujii and Kamachi, 2003; Fujii, 2005)	M1QN3	M1QN3
	Control vector (temporal and sectorial resolution)		annual for 5 categories (anthropogenic emisssions except rice cultivation), monthly for 4 categories (fire, wetland, rice, and soil uptake), climatology for 1 category (termite+geological+ocean)	0.2° × 0.2°, 15 days, 6 categories: gas, coal, agriculture, biofuel, waste, wetlands	

Table S11: Characteristics of the top-down inverse systems contributing to this study. MIROC4-ACTM, NIESMON-CH4, NIES-TM-FLEXPART, and TM5-CAMS. 2/2

		MIROC4-ACTM	NIESMON-CH4	NIES-TM-FLEXPART	TM5-CAMS
Prior sources	Anthropogenic		GCP	GCP	
	Biomass burn.		GCP	GCP	
	Wetlands		GCP	GCP	
	Rice		GCP	GCP	
	Termites		GCP	GCP	
	Other		GCP (geological and oceans)	GCP (geological and oceans)	
Prior sinks	Soil uptake		GCP	GCP	
	Chemistry		OH, O1D, Cl Transcom-CH4 (Patra et al., 2011)	OH, O1D, Cl Transcom-CH4 (Patra et al., 2011)	
Data assimilated	Surface Obs.	NOAA, CSIRO (41 stations)	All data in obspack_ch4_1_GLOBALVIEWplus_v4.0_2021-10-14 (Schuldt et al., 2021), and obspack_ch4_1_NRT_v4.0_2022-03-03 (Schuldt et al., 2021), and additional NIES data (JR-station, HAT, COI, CLA, DMV, NTL, HPP, VOS, MFJ, Mirai)	Obspack, ICOS, "background" sites with max 34 ppb RMSE	NOAA
	Satellite Data	-	-	GOSAT NIES L2 retrieval v02.95 (Yoshida et al., 2013)	GOSAT ESA/CCI product v2.3.8 (Detmers & Hasekamp, 2016, report
	Satellite data processing if any	-	-	bias correction varying by 5 deg latitude band and month	Latitudinal bias correction applied based on the biases between posterior TM5 simulations from the in-situ inversion and the GOSAT product.
Observation errors	Surface observation	Variable model error + 5ppb instrumental error	variable error according to simulated or observed monthly std with deweighting according to the number of observations within a 500 km-radius circle	10 to 44 ppb, depending on sites	Following Bergamaschi et al. (2010)
	Satellite Data	-	-	60 ppb	Combination of GOSAT retrieval and model representation errors.
Time window		Monthly	261 months (Jul 1999 – Mar 2021)	18 month each year (Oct-Mar)	Sequence of 3 yearly inversions (2000-2014) or 1 yearly (2015, 2016,2017) , each with 6 months spin-up/spin-down.
Time period covered		2000-2020	2000-2020	Surface : 2000-2020 Satellite: 2010-2020	Surface : 2000-2020 Satellite: 2010-2020

S8 Comparison of 2000-2009 decadal emissions through the different budgets

Table S12: Global methane emissions by source type for 2000 - 2009 decade ($TgCH_4\,yr^{-1}$)

	Saunois et al. (2016)		Saunois et al. (2020)		This work	
Approach	Bottom-up	Top-down	Bottom-up	Top-down	Bottom-up	Top-down
Natural sources						
Wetlands	183 [151-222]	166 [125-204]	147 [102-179]	180 [153-196]	153 [116-189]	158 [145-172]
Freshwaters	122 [60-180]		209 [134-284]		89 [40-166]	
Other natural sources	199 [104-297]	68 [21-130]	222 [143-306]	35 [21-47]	63 [24-93]	44 [40-46]
Geological	40 [30-56]		38 [13-53]		35 [13-53]	22 [21-25]
Termites	9 [3-15]		9 [3-15]		10 [4-16]	10 [9-11]
Oceanic sources	14 [5-25]		13 [9-22]		13 [6-20]	12 [11-12]
Total natural sources	382 [255-519]	234 [194-292]	369 [245-485]	215 [176-243]	216 [140-282]	204 [189-223]
Anthropogenic sources						
Agriculture and waste	189 [169-205]	183 [112-241]	192 [171-206]	202 [198-219]	195 [175-215]	210 [197-223]
Enteric ferm. & manure	103 [95-109]		104 [93-109]		104 [100-110]	108 [108-108]
Landfills & waste	57 [51-61]		60 [55-63]		61 [52-71]	65 [62-71]
Rice cultivation	29 [23-35]		28 [23-34]		30 [24-34]	35 [34-35]
Fossil fuels	112 [107-126]	101 [77-126]	110 [94-129]	101 [71-151]	105 [97-123]	105 [88-115]
Coal mining	36 [24-43]		32 [24-42]		30 [26-32]	29 [24-32]
Oil & gas	76 [64-85]		73 [60-85]		65 [63-71]	77 [64-90]
Industry			2 [0-6]		4 [1-8]	
Transport			4 [1-11]		3 [1-8]	
Biomass & biofuel burning	30 [26-34]	35 [16-53]	31 [26-46]	29 [23-35]	30 [22-44]	26 [22-29]
Biomass burning	18 [15-20]		19 [15-32]		19 [14-29]	14 [11-16]
Biofuel burning	12 [9-14]		12 [9-14]		11 [8-14]	11 [6-12]
Total anthropogenic sources	338 [329-342]	319 [255-357]	334 [321-358]	332 [312-347]	333 [305-365]	341 [319-355]
Sinks						
Total chemical loss	604 [483-738]	514	595 [489-749]	505 [459-516]		504 [496-511]
Tropospheric OH	528 [454-617]		553 [476-677]			472 [468-477]
Stratospheric loss	51 [16-84]		31 [12-37]			37 [27-51]
Tropospheric Cl	25 [13-37]		32 [27-38]			3 [0-8]
Soil uptake	28 [9-47]	32 [27-38]	30 [11-49]	34 [27-41]	35 [30-38]	34 [34-34]
Total sinks	632 [492-785]	546	625 [500-798]	539 [486-557]		538 [530-545]
Sources - sink imbalance						
Total sources	720 [584-861]	552 [535-566]	703 [566-843]	547 [524-560]	549 [445-647]	543 [526-558]

S9 Regional budgets: Tables and plots

Table S13: USA, Canada, Central America methane emissions by source type ($TgCH_4\,yr^{-1}$)

Region	USA		Canada		Central America	
Approach	Bottom-up	Top-down	Bottom-up	Top-down	Bottom-up	Top-down
Natural sources						
Comb. wetland & inland freshwaters	16 [4-30]	5 [5-6]	30 [10-60]	12 [9-18]	6 [2-14]	4 [4-5]
Wetlands	10 [2-19]		14 [3-26]		4 [1-9]	
Freshwaters	6 [3-12]		17 [7-34]		2 [1-5]	
Other natural sources	8 [3-12]	5 [3-7]	2 [1-3]	1 [1-1]	2 [1-3]	1 [1-2]
Total natural sources	24 [7-43]	12 [7-22]	32 [11-63]	14 [11-22]	8 [3-17]	5 [2-6]
Anthropogenic sources						
Agriculture and waste	14 [12-16]	13 [9-16]	2 [2-3]	2 [1-3]	7 [6-9]	9 [8-10]
Enteric ferm. & manure	9 [7-9]		1 [1-1]		4 [3-5]	
Landfills & waste	5 [4-6]		1 [1-1]		3 [2-4]	
Rice cultivation	0 [0-1]		0 [0-0]		0 [0-0]	
Fossil fuels	11 [4-18]	12 [7-16]	3 [1-4]	4 [2-5]	2 [1-3]	2 [2-3]
Coal mining	3 [2-3]		0 [0-0]		0 [0-0]	
Oil & gas	8 [1-12]		2 [1-4]		1 [1-2]	
Industry	0 [0-1]		0 [0-0]		0 [0-0]	
Transport	0 [0-1]		0 [0-0]		0 [0-0]	
Biomass & biofuel burning	1 [0-1]	1 [0-1]	1 [0-1]	1 [0-1]	1 [0-1]	0 [0-1]
Biomass burning	0 [0-0]		1 [0-1]		0 [0-0]	
Biofuel burning	0 [0-0]		0 [0-0]		0 [0-0]	
Total anthropogenic sources	26 [19-34]	25 [16-31]	6 [3-8]	7 [5-9]	10 [8-12]	12 [11-13]
Total sources	49 [27-77]	38 [32-46]	38 [14-71]	20 [17-24]	18 [10-28]	17 [14-19]

Table S14: Northern South America, Brazil, Southwest South America methane emissions by source type ($TgCH_4\,yr^{-1}$)

Region	Northern South America		Brazil		Southwest South America	
Approach	Bottom-up	Top-down	Bottom-up	Top-down	Bottom-up	Top-down
Natural sources						
Comb. wetland & inland freshwaters	8 [2-15]	8 [6-10]	29 [10-52]	24 [20-33]	18 [5-31]	22 [14-33]
Wetlands	7 [2-11]		25 [8-41]		14 [3-21]	
Freshwaters	1 [0-3]		5 [2-11]		4 [1-9]	
Other natural sources	2 [1-3]	1 [1-2]	3 [1-4]	2 [2-3]	3 [1-4]	2 [2-3]
Total natural sources	10 [3-17]	9 [7-11]	32 [11-57]	26 [22-36]	21 [6-35]	24 [16-34]
Anthropogenic sources						
Agriculture and waste	4 [3-4]	4 [4-5]	16 [14-19]	19 [14-22]	10 [8-12]	12 [9-14]
Enteric ferm. & manure	3 [3-3]		12 [11-13]		7 [6-9]	
Landfills & waste	1 [0-1]		3 [3-5]		2 [1-2]	
Rice cultivation	0 [0-0]		0 [0-1]		0 [0-0]	
Fossil fuels	5 [2-13]	2 [2-3]	1 [0-1]	1 [0-2]	2 [1-3]	2 [1-2]
Coal mining	0 [0-1]		0 [0-0]		0 [0-0]	
Oil & gas	2 [1-2]		0 [0-1]		1 [1-2]	
Industry	0 [0-0]		0 [0-1]		0 [0-0]	
Transport	0 [0-0]		0 [0-0]		0 [0-0]	
Biomass & biofuel burning	0 [0-0]	0 [0-0]	1 [1-2]	1 [1-2]	1 [1-1]	1 [1-1]
Biomass burning	0 [0-0]		1 [1-1]		1 [1-1]	
Biofuel burning	0 [0-0]		0 [0-0]		0 [0-0]	
Total anthropogenic sources	9 [6-17]	7 [6-8]	19 [16-22]	21 [17-26]	13 [10-16]	14 [12-17]
Total sources	19 [9-35]	16 [13-20]	51 [26-79]	47 [41-58]	34 [16-51]	38 [30-48]

Table S15: Europe, Northern Africa, Equatorial Africa methane emissions by source type ($TgCH_4\,yr^{-1}$)

Region	Europe		Northern Africa		Equatorial Africa	
Approach	Bottom-up	Top-down	Bottom-up	Top-down	Bottom-up	Top-down
Natural sources						
Comb. wetland & inland freshwaters	9 [3-17]	2 [2-2]	6 [2-11]	5 [4-7]	21 [9-45]	22 [19-28]
Wetlands	5 [1-9]		2 [0-4]		14 [6-31]	
Freshwaters	4 [2-8]		3 [1-7]		7 [3-15]	
Other natural sources	8 [3-13]	6 [3-7]	1 [0-2]	1 [1-1]	2 [1-3]	2 [1-2]
Total natural sources	17 [6-30]	7 [5-9]	7 [2-13]	6 [6-8]	23 [10-49]	24 [20-30]
Anthropogenic sources						
Agriculture and waste	19 [17-23]	19 [16-23]	11 [4-15]	13 [12-14]	11 [7-15]	13 [11-15]
Enteric ferm. & manure	11 [10-12]		7 [2-10]		6 [5-7]	
Landfills & waste	8 [6-12]		3 [2-4]		3 [2-4]	
Rice cultivation	0 [0-0]		0 [0-1]		2 [1-3]	
Fossil fuels	5 [3-6]	4 [2-7]	6 [5-7]	5 [4-7]	7 [4-8]	6 [3-10]
Coal mining	2 [1-2]		0 [0-0]		0 [0-0]	
Oil & gas	2 [0-4]		5 [4-5]		5 [2-8]	
Industry	0 [0-1]		0 [0-1]		0 [0-2]	
Transport	0 [0-0]		0 [0-0]		0 [0-0]	
Biomass & biofuel burning	1 [0-1]	1 [1-1]	1 [0-2]	1 [1-1]	5 [3-8]	5 [4-5]
Biomass burning	0 [0-0]		0 [0-1]		2 [2-3]	
Biofuel burning	1 [0-1]		1 [1-1]		2 [2-2]	
Total anthropogenic sources	25 [22-27]	24 [20-31]	18 [16-20]	19 [17-21]	24 [19-34]	23 [19-29]
Total sources	42 [29-57]	31 [24-36]	24 [18-33]	25 [23-29]	47 [28-83]	47 [39-59]

Table S16: Southern Africa, Russia, Central Asia methane emissions by source type ($TgCH_4\,yr^{-1}$)

Region	Southern Africa		Russia		Central Asia	
Approach	Bottom-up	Top-down	Bottom-up	Top-down	Bottom-up	Top-down
Natural sources						
Comb. wetland & inland freshwaters	10 [2-27]	7 [4-9]	22 [7-41]	11 [8-13]	7 [2-19]	1 [1-1]
Wetlands	6 [-0-18]		13 [4-23]		0 [-0-2]	
Freshwaters	4 [2-9]		9 [4-18]		7 [2-17]	
Other natural sources	1 [1-2]	1 [1-1]	4 [2-6]	3 [1-4]	1 [0-1]	1 [0-1]
Total natural sources	11 [2-29]	8 [7-10]	25 [9-47]	14 [11-18]	8 [2-19]	1 [0-2]
Anthropogenic sources						
Agriculture and waste	5 [1-8]	5 [4-6]	5 [5-6]	5 [3-6]	3 [2-3]	3 [2-5]
Enteric ferm. & manure	2 [1-3]		2 [2-2]		2 [1-3]	
Landfills & waste	2 [0-5]		3 [3-4]		1 [0-1]	
Rice cultivation	0 [0-0]		0 [0-0]		0 [0-0]	
Fossil fuels	3 [1-4]	4 [3-4]	15 [9-27]	14 [8-23]	5 [3-6]	5 [4-7]
Coal mining	1 [0-2]		3 [2-4]		1 [1-1]	
Oil & gas	1 [0-3]		12 [6-24]		3 [1-5]	
Industry	0 [0-1]		0 [0-2]		0 [0-0]	
Transport	0 [0-0]		0 [0-0]		0 [0-0]	
Biomass & biofuel burning	3 [1-4]	3 [2-3]	2 [1-4]	2 [1-2]	0 [0-0]	0 [0-0]
Biomass burning	2 [1-3]		1 [1-3]		0 [0-0]	
Biofuel burning	0 [0-1]		0 [0-0]		0 [0-0]	
Total anthropogenic sources	10 [3-14]	11 [10-12]	23 [15-36]	21 [14-29]	8 [4-10]	9 [7-11]
Total sources	21 [5-43]	19 [16-24]	48 [24-83]	36 [27-45]	15 [6-29]	10 [8-13]

Table S17: Middle East, China, Korean Japan methane emissions by source type ($TgCH_4\,yr^{-1}$)

Region	Middle East		China		Korean Japan	
Approach	Bottom-up	Top-down	Bottom-up	Top-down	Bottom-up	Top-down
Natural sources						
Comb. wetland & inland freshwaters	4 [1-8]	1 [0-1]	12 [3-30]	3 [2-4]	1 [0-5]	0 [0-1]
Wetlands	1 [0-1]		7 [1-18]		1 [0-4]	
Freshwaters	3 [1-7]		5 [2-12]		0 [0-1]	
Other natural sources	5 [2-7]	3 [1-5]	2 [1-4]	1 [0-2]	1 [0-2]	1 [1-1]
Total natural sources	9 [3-15]	4 [1-6]	15 [4-33]	4 [3-7]	3 [1-7]	1 [1-1]
Anthropogenic sources						
Agriculture and waste	9 [7-10]	10 [9-11]	32 [19-44]	30 [13-36]	3 [2-4]	4 [3-4]
Enteric ferm. & manure	3 [2-4]		11 [8-16]		1 [1-1]	
Landfills & waste	5 [4-6]		11 [6-14]		1 [1-1]	
Rice cultivation	0 [0-0]		9 [5-14]		1 [1-1]	
Fossil fuels	17 [9-21]		24 [23-26]		1 [0-1]	
Coal mining	0 [0-0]		21 [20-21]		0 [0-1]	
Oil & gas	16 [8-20]		2 [2-2]		0 [0-0]	
Industry	0 [0-0]		1 [0-1]		0 [0-0]	
Transport	0 [0-0]		0 [0-1]		0 [0-0]	
Biomass & biofuel burning	0 [0-0]	0 [0-0]	2 [1-4]	3 [0-4]	0 [0-0]	0 [0-0]
Biomass burning	0 [0-0]		0 [0-1]		0 [0-0]	
Biofuel burning	0 [0-0]		2 [1-3]		0 [0-0]	
Total anthropogenic sources	26 [18-31]	28 [20-34]	57 [51-66]	53 [34-66]	4 [3-5]	4 [3-5]
Total sources	35 [21-47]	31 [24-39]	71 [55-99]	57 [37-72]	6 [4-12]	5 [4-6]

Table S18: South Asia, Southeast Asia, Australasia methane emissions by source type ($TgCH_4\,yr^{-1}$)

Region	South Asia		Southeast Asia		Australasia	
Approach	Bottom-up	Top-down	Bottom-up	Top-down	Bottom-up	Top-down
Natural sources						
Comb. wetland & inland freshwaters	12 [5-23]	5 [4-6]	27 [17-45]	24 [14-29]	7 [3-15]	4 [4-5]
Wetlands	9 [3-17]		24 [16-38]		3 [1-6]	
Freshwaters	3 [1-6]		3 [1-7]		4 [2-9]	
Other natural sources	1 [0-2]	1 [1-1]	6 [2-9]	4 [2-6]	3 [1-4]	2 [2-2]
Total natural sources	13 [5-25]	6 [5-6]	32 [19-54]	27 [20-34]	10 [4-19]	6 [4-7]
Anthropogenic sources						
Agriculture and waste	37 [26-45]	39 [33-43]	19 [14-25]	24 [21-31]	5 [4-5]	4 [4-5]
Enteric ferm. & manure	20 [18-22]		4 [3-5]		4 [3-4]	
Landfills & waste	9 [4-11]		6 [4-8]		1 [1-1]	
Rice cultivation	8 [5-12]		9 [8-12]		0 [0-0]	
Fossil fuels	4 [4-5]	4 [3-4]	8 [5-10]	8 [6-11]	2 [1-2]	2 [1-2]
Coal mining	2 [1-3]		5 [4-5]		1 [1-1]	
Oil & gas	1 [1-2]		3 [1-4]		0 [0-0]	
Industry	0 [0-1]		0 [0-1]		0 [0-0]	
Transport	0 [0-0]		0 [0-0]		0 [0-0]	
Biomass & biofuel burning	3 [2-3]	2 [2-3]	5 [2-7]	4 [2-5]	1 [0-1]	1 [0-1]
Biomass burning	0 [0-1]		4 [1-6]		1 [0-1]	
Biofuel burning	2 [2-3]		1 [0-1]		0 [0-0]	
Total anthropogenic sources	45 [44-47]	45 [38-49]	32 [23-39]	35 [31-46]	7 [6-7]	7 [6-7]
Total sources	58 [49-72]	52 [43-60]	64 [42-93]	63 [52-71]	16 [9-26]	13 [10-17]

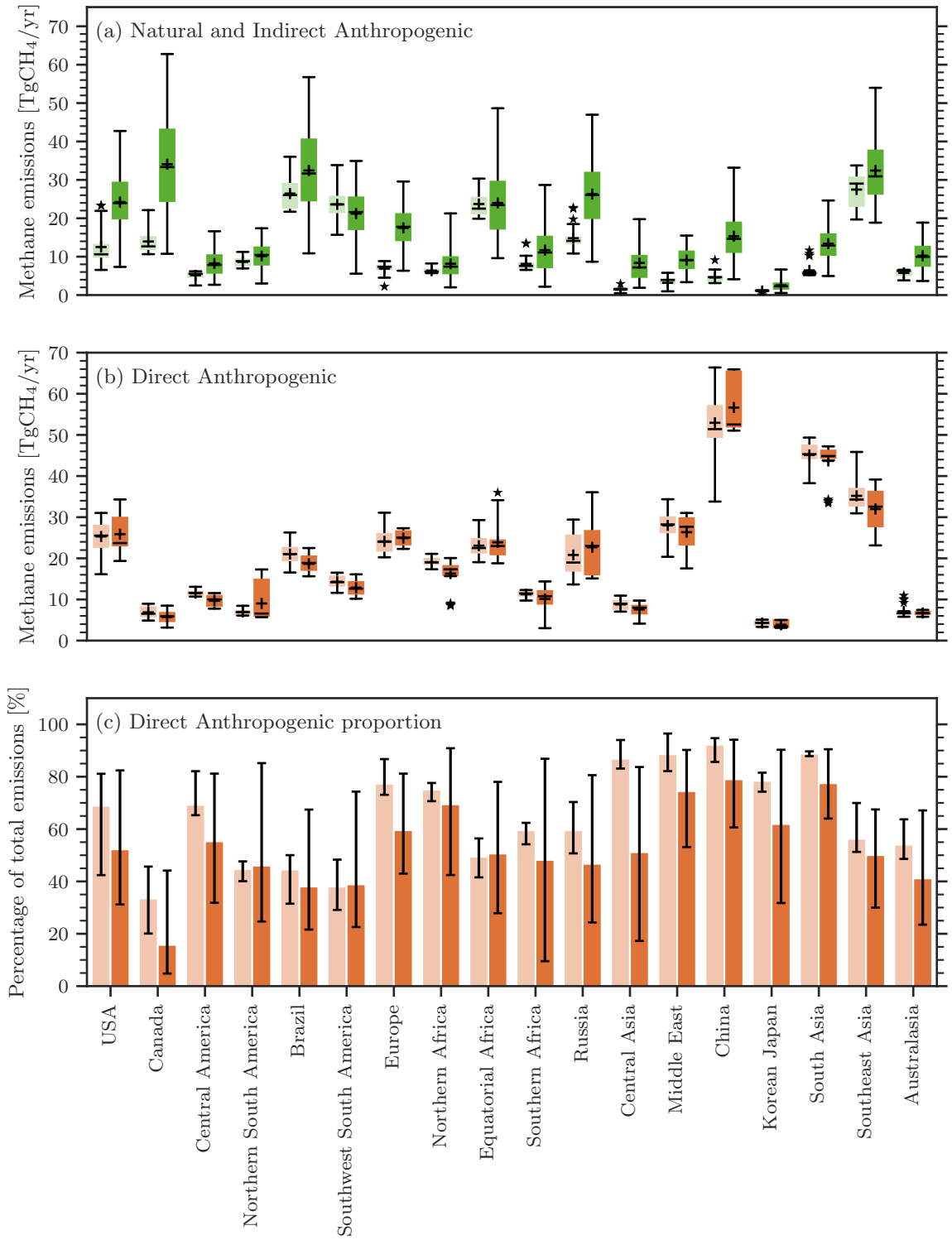

Figure S5: (a) Natural (green) emissions by region, (b) mean anthropogenic (orange), and (c) mean anthropogenic proportion as a percentage of total regional emissions (orange) in $TgCH_4\,yr^{-1}$ for 2010 – 2019 decade for top-down estimates (left light colored box plots or bars) and bottom-up estimates (right dark colored box plots or bars). Suspected outliers are marked with stars in (a) and (b) and excluded from (c), they were determined as values below the first quartile minus 3 times the inter-quartile range, or values above the third quartile plus 3 times the inter-quartile range. Mean values are represented with "+" symbols.

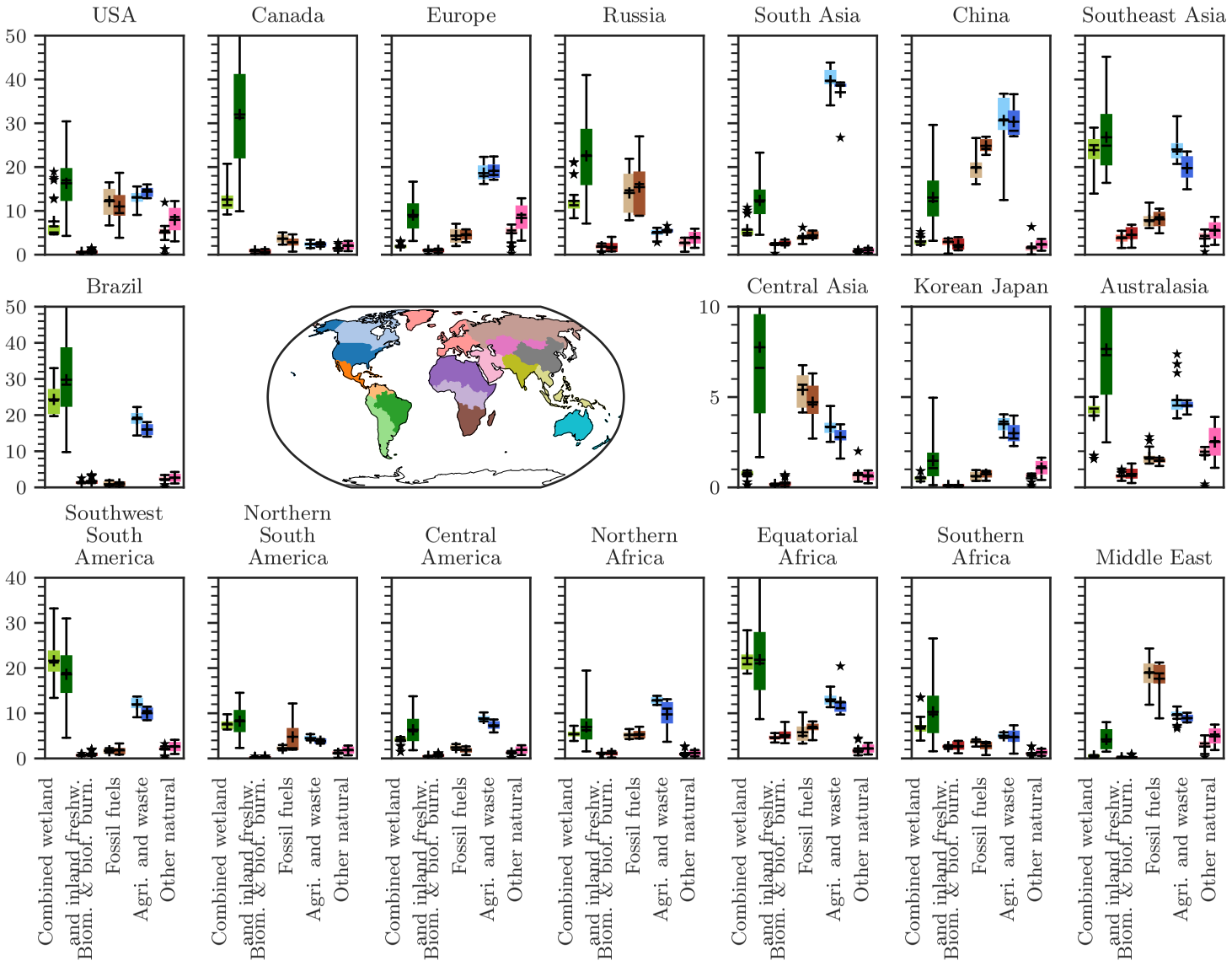

Figure S6: Regional emissions for main emissions broad categories: inland waters, fossil fuel and agriculture Waste, Biomass and Biofuel burning and Other natural emissions from top-down estimates (left boxplots and bottom-up estimates (right boxplots). The inner map shows the region's distribution. Values are given for the 2010-2019 decade.

S10 Methane recent changes

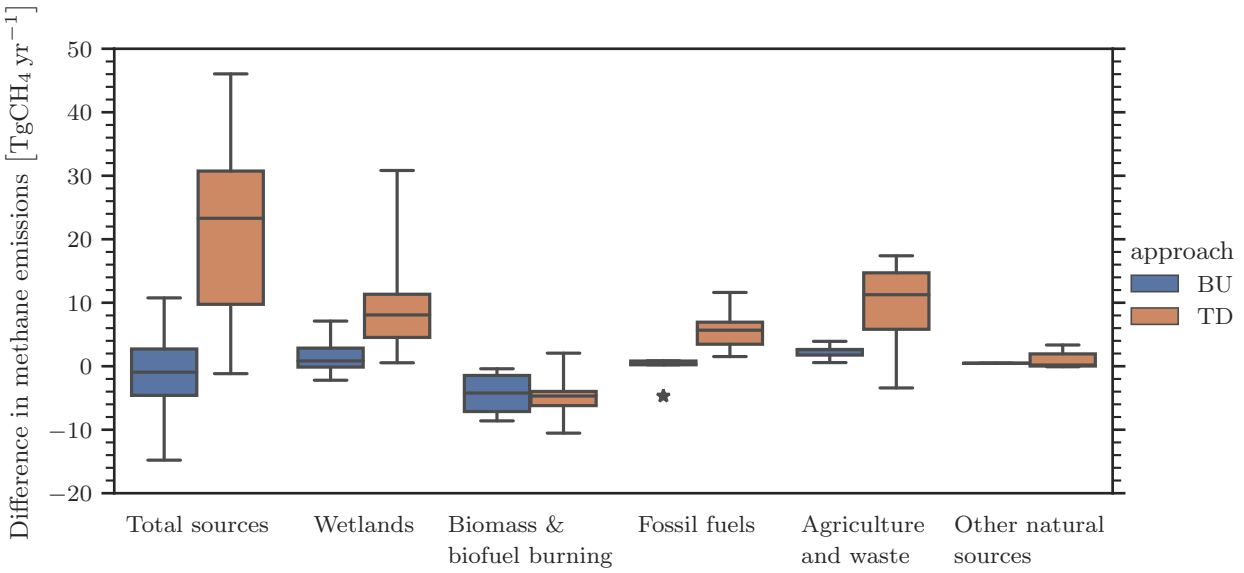

Figure S7: Difference in global emissions between 2020 and 2019 based on the ensemble of data sets contributing the bottom-up and top-down budgets.

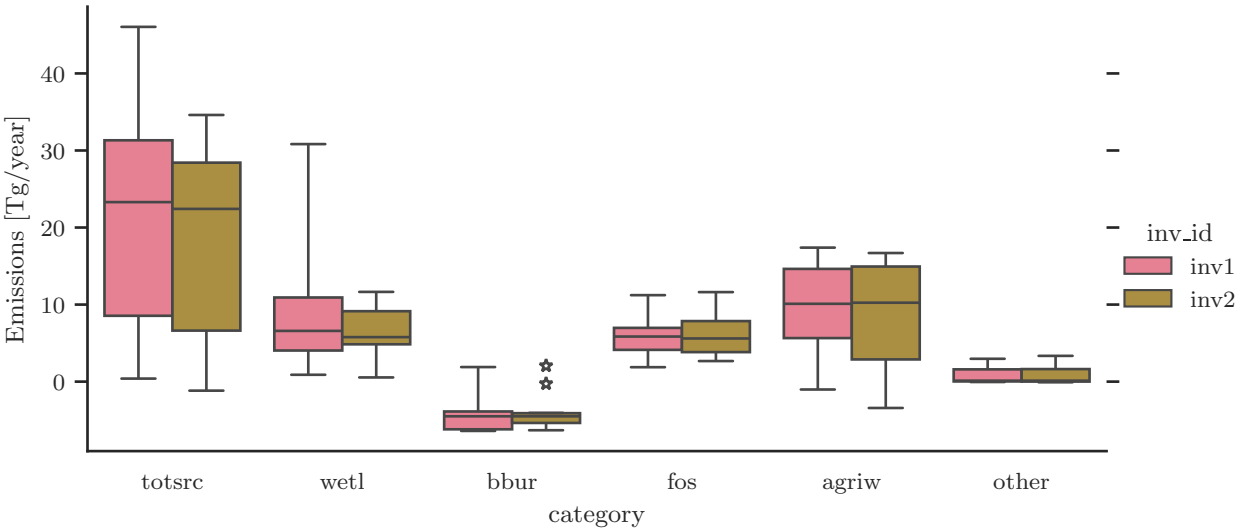

Figure S8: Difference in global emissions between 2020 and 2019 based on the top-down approaches only, for the total sources (totsrc) and wetland (wetl), biomass and biofuel burning (bbur), fossil fuels (fos), agriculture and waste (agriw), and other natural (other) emissions. Inv1 group assumed constant OH through the full period of inversion. Inv2 group assumed OH IAV based on Patra et al., (2021).

Table S19: Direct anthropogenic emissions estimated by EDGARv8 inventory for years 2020 to 2022 in $TgCH_4\,yr^{-1}$

	2020	2021	2022	Difference 2022-2020
Total anthropogenic emissions	373.7	379.4	386.0	12.3
Fossil fuel total	118.6	121.6	126.2	7.6
Coal	42.2	43.5	46.8	
Oil and gas	67.7	68.5	69.8	
Industry	8.2	8.4	8.4	
Transport	1.0	1.0	1.1	
Agriculture and waste total	243.9	246.6	248.5	4.6
Agriculture total	159.8	160.9	161.5	1.7
Livestock	123.0	124.1	125.0	
Rice	36.8	36.9	36.5	
Landfill and waste	84.1	85.6	87.0	2.9
Biofuel	11.3	11.3	11.3	

S11 TROPOMI - observations

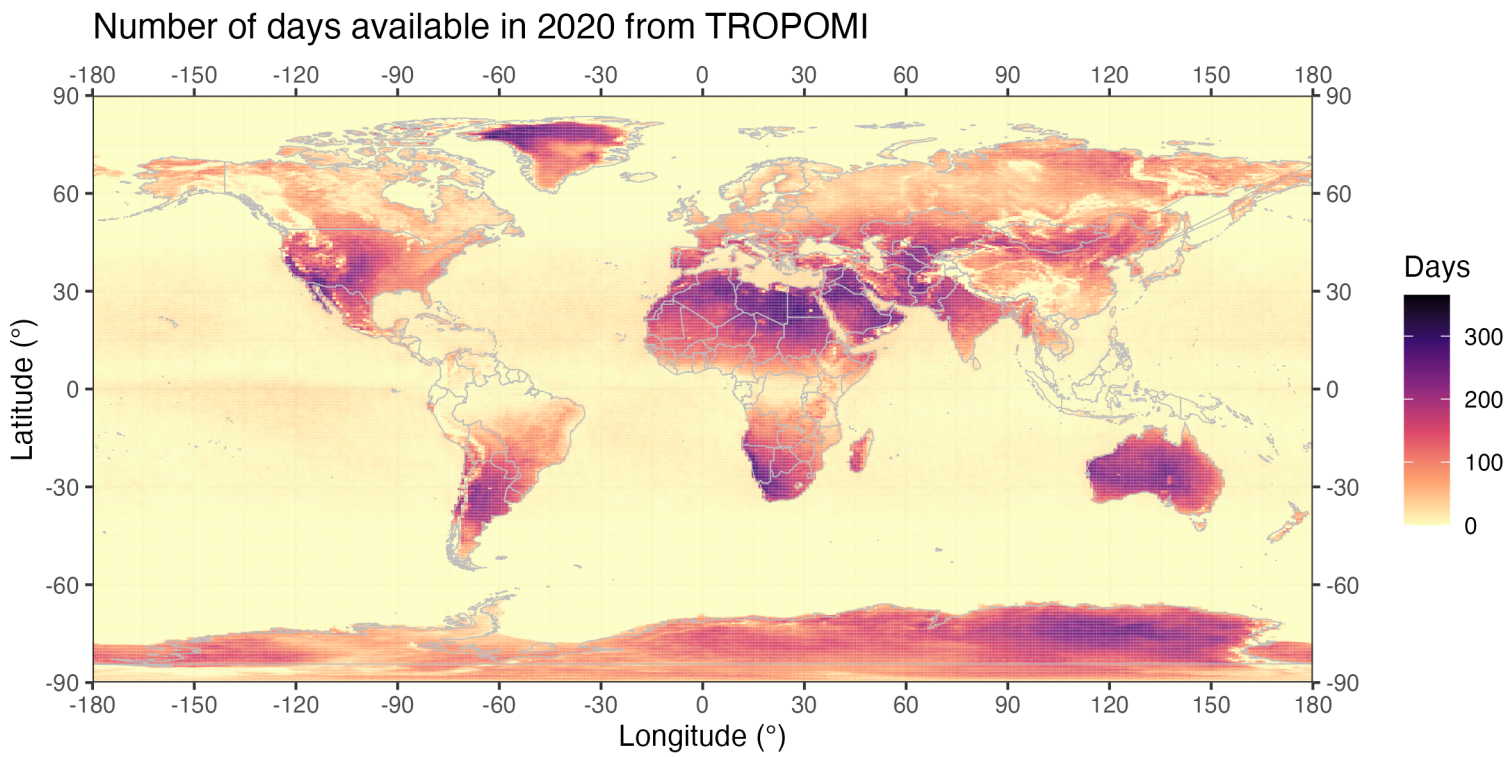

Figure S9: Number of daily observations over the year 2020 from the product Sentinel-5P TROPOMI Methane CH4 L2 5.5km x 7km, last access date Dec 1, 2023 via NASA: `https://disc.gsfc.nasa.gov/datasets/S5P_L2__CH4____HiR_2/summary?keywords=tropomi%20ch4`.

References

Arakawa, A. and Schubert, W. H.: Interactions of cu- mulus cloud ensemble with the large-scale environment, Part I, J. Atmos. Sci., 31, 674–701, doi:10.1175/1520- 0469(1974)031¡0674:IOACCE¿2.0.CO;2, 1974.

Bergamaschi, P., Krol, M., Meirink, J. F., Dentener, F., Segers, A., van Aardenne, J., Monni, S., Vermeulen, A. T., Schmidt, M., Ramonet, M., Yver, C., Meinhardt, F., Nisbet, E. G., Fisher, R. E., O'Doherty, S., and Dlugokencky, E. J.: Inverse modeling of European CH4 emissions 2001–2006, J. Geophys. Res.-Atmos., 115, D22309, https://doi.org/10.1029/2010JD014180, 2010.

Bergamaschi, P., Houweling, S., Segers, A., Krol, M., Frankenberg, C., Scheepmaker, R. A., Dlugokencky, E., Wofsy, S. C., Kort, E. A., Sweeney, C., Schuck, T., Brenninkmeijer, C., Chen, H., Beck, V., and Gerbig, C.: Atmospheric CH4 in the first decade of the 21st century: Inverse modeling analysis using SCIAMACHY satellite retrievals and NOAA surface measurements, J. Geophys. Res.-Atmos., 118, 7350–7369, https://doi.org/10.1002/jgrd.50480, 2013.

Chen, Y. H. and Prinn, R. G.: Estimation of atmospheric methane emissions between 1996 and 2001 using a three-dimensional global chemical transport model, J. Geophys. Res.-Atmos., 111, D10307, doi:10.1029/2005JD006058, 2006.

Chevallier, F., Fisher, M., Peylin, P., Serrar, S., Bousquet, P., Breon, F. M., Chedin, A., and Ciais, P.: Inferring CO2 sources and sinks from satellite observations: Method and applica- tion to TOVS data, J. Geophys. Res.-Atmos., 110, D24309, doi:10.1029/2005jd006390, 2005.

Chevallier, F., Bréon, F. M., and Rayner, P. J.: Contribution of the Orbiting Carbon Observatory to the estimation of CO2 sources and sinks: Theoretical study in a variational data as- similation framework, J. Geophys. Res.-Atmos., 112, D09307, doi:10.1029/2006jd007375, 2007.

Chikira, M., Sugiyama, M.: A cumulus parameterization with state-dependent entrainment rate. Part I: Description and sensitivity to temperature and humidity profiles. Journal of the Atmospheric Sciences, 67(7), 2171-2193, 2010

Collins, W. J., Lamarque, J. F., Schulz, M., Boucher, O., Eyring, V, Hegglin, M. I., Maycock, A., Myhre, G., Prather, M., Shindell, D. and Smith, S.J.: AerChemMIP: quantifying the effects of chemistry and aerosols in CMIP6. Geoscientific Model Development 10, 585–607. doi:10.5194/ gmd-10-585-2017, 2017.

Crippa, M., Guizzardi, D., Solazzo, E., Muntean, M., Schaaf, E., Monforti-Ferrario, F., Banja, M., Olivier, J.G.J., Grassi, G., Rossi, S., Vignati, E.,GHG emissions of all world countries - 2021 Report, EUR 30831 EN, Publications Office of the European Union, Luxembourg, 2021, ISBN 978-92-76-41547-3, doi:10.2760/173513, JRC126363, 2021

Curry, C. L.: Modeling the soil consumption of atmospheric methane at the global scale, Glob. Biogeochem. Cycles, 21(4), GB4012, doi:10.1029/2006gb002818, 2007.

Dutaur, L. and Verchot, L. V.: A global inventory of the soil CH4 sink, Global Biogeochem. Cy., 21, GB4012, doi:10.1029/2006GB002734, 2007.

Etiope, G., Ciotoli, G., Schwietzke, S. and Schoell, M.: Gridded maps of geological methane emissions and their isotopic signature, Earth Syst Sci Data, 11(1), 1–22, doi:10.5194/essd-11-1-2019, 2019.

Fujii Y, Kamachi M: A nonlinear preconditioned quasi-newton method without inversion of a first-guess covariance matrix in variational analyses. Tellus A 55(5):450–454. https://doi.org/10.1034/j.1600-0870.2003.00030, 2003

Fujii Y: Preconditioned optimizing utility for large-dimensional analyses (POpULar). J Oceanogr 61(1):167–181. https://doi.org/10.1007/s10872-005-0029-z, 2005

Gregory, D., Morcrette, J.-J., Jakob, C., Beljaars, A. C. M., and Stockdale, T.: Revision of convection, radiation and cloud schemes in the ECMWF integrated forecasting system, Q. J. Roy. Meteorol. Soc., 126, 1685–1710, doi:10.1002/qj.49712656607, 2000.

Harada Y, Kamahori H, Kobayashi C, Endo H, Kobayashi S, Ota Y, Onoda H, Onogi K, Miyaoka K, Takahashi K: The JRA-55 reanalysis: representation of atmospheric circulation and climate variability. J Meteor Soc Jpn 94(3):269–302. https://doi.org/10.2151/jmsj.2016-015, 2016

Hmiel, B., Petrenko, V. V., Dyonisius, M. N., Buizert, C., Smith, A. M., Place, P. F., Harth, C., Beaudette, R., Hua, Q., Yang, B., Vimont, I., Michel, S. E., Severinghaus, J. P., Etheridge, D., Bromley, T., Schmitt, J., Faïn, X., Weiss, R. F. and Dlugokencky, E.: Preindustrial 14 CH 4 indicates greater anthropogenic fossil CH 4 emissions, Nature, 578(7795), 409–412, doi:10.1038/s41586-020-1991-8, 2020.

Holtslag, A. A. M., Boville, B. A.: Local versus nonlocal boundary-layer diffusion in a global climate model. Journal of climate, 6(10), 1825-1842, 1993

Ito, A. and Inatomi, M.: Use of a process-based model for assessing the methane budgets of global terrestrial ecosystems and evaluation of uncertainty, Biogeosciences, 9(2), 759–773, doi:10.5194/bg-9-759-2012, 2012.

Kaiser, S., Göckede, M., Castro-Morales, K., Knoblauch, C., Ekici, A., Kleinen, T., Zubrzycki, S., Sachs, T., Wille, C., and Beer, C.: Process-based modelling of the methane balance in periglacial landscapes (JSBACH-methane), Geosci. Model Dev., 10, 333–358, https://doi.org/10.5194/gmd-10-333-2017, 2017.

Kaminski, T., Rayner, P. J., Heimann, M., and Enting, I. G.: On ag- gregation errors in atmospheric transport inversions, J. Geophys. Res.-Atmos., 106, 4703–4715, 2001.

Kirschke, S., Bousquet, P., Ciais, P., Saunois, M., Canadell, J. G., Dlugokencky, E. J., Bergamaschi, P., Bergmann, D., Blake, D. R., Bruhwiler, L., Cameron-Smith, P., Castaldi, S., Chevallier, F., Feng, L., Fraser, A., Heimann, M., Hodson, E. L., Houwel- ing, S., Josse, B., Fraser, P. J., Krummel, P. B., Lamarque, J. F., Langenfelds, R. L., Le Quere, C., Naik, V., O'Doherty, S., Palmer, P. I., Pison, I., Plummer, D., Poulter, B., Prinn, R. G., Rigby, M., Ringeval, B., Santini, M., Schmidt, M., Shindell, D. T., Simpson, I. J., Spahni, R., Steele, L. P., Strode, S. A., Sudo, K., Szopa, S., van der Werf, G. R., Voulgarakis, A., van Weele, M., Weiss, R. F., Williams, J. E., and Zeng, G.: Three decades of global methane sources and sinks, Nat. Geosci., 6, 813–823, doi:10.1038/ngeo1955, 2013.

Kobayashi S, Ota Y, Harada Y, Ebita A, Moriya M, Onoda H, Onogi K, Kamahori H, Kobayashi C, Endo H, Miyaoka K, Takahashi K : The JRA-55 reanalysis: general specifications and basic characteristics. J Meteorol Soc Japan Ser II 93(1):5–48. https://doi.org/10.2151/jmsj.2015-001, 2015

Krol, M., de Bruine, M., Killaars, L., Ouwersloot, H., Pozzer, A., Yin, Y., Chevallier, F., Bousquet, P., Patra, P., Belikov, D., Maksyutov, S., Dhomse, S., Feng, W., and Chipperfield, M. P.: Age of air as a diagnostic for transport timescales in global models, Geosci. Model Dev., 11, 3109–3130, https://doi.org/10.5194/gmd-11-3109-2018, 2018.

Maksyutov, S., Oda, T., Saito, M., Janardanan, R., Belikov, D., Kaiser, J. W., Zhuravlev, R., Ganshin, A., Valsala, V. K., Andrews, A., Chmura, L., Dlugokencky, E., Haszpra, L., Langenfelds, R. L., Machida, T., Nakazawa, T., Ramonet, M., Sweeney, C., and Worthy, D.: Technical note: A high-resolution inverse modelling technique for estimating surface CO2 fluxes based on the NIES-TM–FLEXPART coupled transport model and its adjoint, Atmos. Chem. Phys., 21, 1245–1266, https://doi.org/10.5194/acp-21-1245-2021, 2021.

Meirink, J. F., Bergamaschi, P., and Krol, M. C.: Four- dimensional variational data assimilation for inverse modelling of atmospheric methane emissions: method and comparison with synthesis inversion, Atmos. Chem. Phys., 8, 6341–6353, doi:10.5194/acp-8-6341-2008, 2008b.

Mellor, G. L. and Yamada, T.: A hierarchy of turbulence closure models for planetary boundary layers, J. Atmos. Sci., 31, 1791– 1806, doi:10.1175/1520-0469 031¡1791:AHOTCM¿2.0.CO;2, 1974.

Mellor, G. L. and Yamada, T.: Development of a turbulence closure model for geostrophic fluid problems, Rev. Geophys., 20, 851– 875, doi:10.1029/RG020i004p00851, 1982.

Murguia-Flores, F., Arndt, S., Ganesan, A. L., Murray-Tortarolo, G. and Hornibrook, E. R. C.: Soil Methanotrophy Model (MeMo v1.0): a process-based model to quantify global uptake of atmospheric methane by soil, Geosci. Model Dev., 11(6), 2009–2032, doi:10.5194/gmd-11-2009-2018, 2018.

Nakanishi, M., Niino, H.: An improved Mellor–Yamada level-3 model with condensation physics: Its design and verification. Boundary-layer meteorology, 112, 1-31, 2004

Niwa, Y., Ishijima, K., Ito, A. and Iida, Y.: Toward a long-term atmospheric CO2 inversion for elucidating natural carbon fluxes: technical notes of NISMON-CO2 v2021.1. Prog. Earth Planet Sci. 9, 42, doi:10.1186/s40645-022-00502-6, 2022

Oreggioni, G. D., F. Monforti Ferrario, M. Crippa, M. Muntean, E. Schaaf, D. Guizzardi, E. Solazzo, M. Duerr, M. Perry and E. Vignati: Climate change in a changing world: Socio-economic and technological transitions, regulatory frameworks and trends on global greenhouse gas emissions from EDGAR v.5.0, Global Environmental Change, doi:10.1016/j.gloenvcha.2021.10235, 2021

Pandey, S., Houweling, S., Krol, M., Aben, I., Chevallier, F., Dlugokencky, E. J., Gatti, L. V., Gloor, M., Miller, J. B., Detmers, R., Machida, T. and Röckmann, T.: Inverse modeling of GOSAT-retrieved ratios of total column CH4 and CO2 for 2009 and 2010, Atmospheric Chem. Phys. Discuss., 2016, 1–32, doi:10.5194/acp-2016-77, 2016.

Patra, P. K., Houweling, S., Krol, M., Bousquet, P., Belikov, D., Bergmann, D., Bian, H., Cameron-Smith, P., Chipperfield, M. P., Corbin, K., Fortems-Cheiney, A., Fraser, A., Gloor, E., Hess, P., Ito, A., Kawa, S. R., Law, R. M., Loh, Z., Maksyutov, S., Meng, L., Palmer, P. I., Prinn, R. G., Rigby, M., Saito, R. and Wilson, C.: TransCom model simulations of CH4 and related species: linking transport, surface flux and chemical loss with CH4 variability in the troposphere and lower stratosphere, Atmospheric Chem. Phys., 11(24), 12,813-12,837, doi:10.5194/acp-11-12813-2011, 2011.

Patra, P. K., Takigawa, M., Watanabe, S., Chandra, N., Ishijima, K. and Yamashita, Y.: Improved Chemical Tracer Simulation by MIROC4.0-based Atmospheric Chemistry-Transport Model (MIROC4-ACTM), SOLA, 14(0), 91–96, doi:10.2151/sola.2018-016, 2018.

Plummer, D., Nagashima, T., Tilmes, S., Archibald, A., Chiodo, G., Fadnavis, S., Garny, H., Josse, B., Kim, J., Lamarque, J.-F., Morgenstern, O., Murray, L., Orbe, C., Tai, A., Chipperfield, M., Funke, B., Juckes, M., Kinnison, D., Kunze, M., Luo, B., Matthes, K., Newman, P. A., Pascoe, C. and Peter, T.: CCMI- 2022: a new set of Chemistry–Climate Model Initiative (CCMI) community simulations to update the assessment of models and support upcoming ozone assessment activities. SPARC Newsletter 57, 22–30, 2021.

Poulter, B., Bousquet, P., Canadell, J. G., Ciais, P., Peregon, A., Saunois, M., Arora, V. K., Beerling, D. J., Brovkin, V., Jones, C. D., Joos, F., Gedney, N., Ito, A., Kleinen, T., Koven, C. D., McDonald, K., Melton, J. R., Peng, C. H., Peng, S. S., Prigent, C., Schroeder, R., Riley, W. J., Saito, M., Spahni, R., Tian, H. Q., Taylor, L., Viovy, N., Wilton, D., Wiltshire, A., Xu, X. Y., Zhang, B. W., Zhang, Z., and Zhu, Q. A.: Global wetland contribution to 2000–2012 atmospheric methane growth rate dynamics, Environ. Res. Lett., 12, 094013, https://doi.org/10.1088/1748-9326/aa8391, 2017.

Ridgwell, A. J., Marshall, S. J. and Gregson, K.: Consumption of atmospheric methane by soils: A process-based model, Glob. Biogeochem. Cycles, 13(1), 59–70, doi:10.1029/1998gb900004, 1999.

Riley, W. J., Subin, Z. M., Lawrence, D. M., Swenson, S. C., Torn, M. S., Meng, L., Mahowald, N. M. and Hess, P.: Barriers to predicting changes in global terrestrial methane fluxes: analyses using CLM4Me, a methane biogeochemistry model integrated in CESM, Biogeosciences, 8(7), 1925–1953, doi:10.5194/bg-8-1925-2011, 2011.

Rodgers, C. D.: Inverse methods for atmospheric sounding: the- ory and practice, Atmospheric, Oceanic and Planetary Physics, edited by: World-Scientific, Singapore, London, 240 pp., 2000.

Saunois, M., Bousquet, P., Poulter, B., Peregon, A., Ciais, P., Canadell, J. G., Dlugokencky, E. J., Etiope, G., Bastviken, D., Houweling, S., Janssens-Maenhout, G., Tubiello, F. N., Castaldi, S., Jackson, R. B., Alexe, M., Arora, V. K., Beerling, D. J., Bergamaschi, P., Blake, D. R., Brailsford, G., Brovkin, V., Bruhwiler, L., Crevoisier, C., Crill, P., Covey, K., Curry, C., Frankenberg, C., Gedney, N., Höglund-Isaksson, L., Ishizawa, M., Ito, A., Joos, F., Kim, H.-S., Kleinen, T., Krummel, P., Lamarque, J.-F., Langenfelds, R., Locatelli, R., Machida, T., Maksyutov, S., McDonald, K. C., Marshall, J., Melton, J. R., Morino, I., Naik, V., O'Doherty, S., Parmentier, F.-J. W., Patra, P. K., Peng, C., Peng, S., Peters, G. P., Pison, I., Prigent, C., Prinn, R., Ramonet, M., Riley, W. J., Saito, M., Santini, M., Schroeder, R., Simpson, I. J., Spahni, R., Steele, P., Takizawa, A., Thornton, B. F., Tian, H., Tohjima, Y., Viovy, N., Voulgarakis, A., van Weele, M., van der Werf, G. R., Weiss, R., Wiedinmyer, C., Wilton, D. J., Wiltshire, A., Worthy, D., Wunch, D., Xu, X., Yoshida, Y., Zhang, B., Zhang, Z., and Zhu, Q.: The global methane budget 2000–2012, Earth Syst. Sci. Data, 8, 697–751, https://doi.org/10.5194/essd-8-697-2016, 2016.

Saunois, M., Stavert, A. R., Poulter, B., Bousquet, P., Canadell, J. G., Jackson, R. B., Raymond, P. A., Dlugokencky, E. J., Houweling, S., Patra, P. K., Ciais, P., Arora, V. K., Bastviken, D., Bergamaschi, P., Blake, D. R., Brailsford, G., Bruhwiler, L., Carlson, K. M., Carrol, M., Castaldi, S., Chandra, N., Crevoisier, C., Crill, P. M., Covey, K., Curry, C. L., Etiope, G., Frankenberg, C., Gedney, N., Hegglin, M. I., Höglund-Isaksson, L., Hugelius, G., Ishizawa, M., Ito, A., Janssens-Maenhout, G., Jensen, K. M., Joos, F., Kleinen, T., Krummel, P. B., Langenfelds, R. L., Laruelle, G. G., Liu, L., Machida, T., Maksyutov, S., McDonald, K. C., McNorton, J., Miller, P. A., Melton, J. R., Morino, I., Müller, J., Murguia-Flores, F., Naik, V., Niwa, Y., Noce, S., O'Doherty, S., Parker, R. J., Peng, C., Peng, S., Peters, G. P., Prigent, C., Prinn, R., Ramonet, M., Regnier, P., Riley, W. J., Rosentreter, J. A., Segers, A., Simpson, I. J., Shi, H., Smith, S. J., Steele, L. P., Thornton, B. F., Tian, H., Tohjima, Y., Tubiello, F. N., Tsuruta, A., Viovy, N., Voulgarakis, A., Weber, T. S., van Weele, M., van der Werf, G. R., Weiss, R. F., Worthy, D., Wunch, D., Yin, Y., Yoshida, Y., Zhang, W., Zhang, Z., Zhao, Y., Zheng, B., Zhu, Q., Zhu, Q., and Zhuang, Q.: The Global Methane Budget 2000–2017, Earth Syst. Sci. Data, 12, 1561–1623, https://doi.org/10.5194/essd-12-1561-2020, 2020.

Schuldt, K. N., Aalto, T., Andrews, A., Aoki, S., Arduini, J., Baier, B., Bergamaschi, P., Biermann, T., Biraud, S. C., Boenisch, H., Brailsford, G., Chen, H., Colomb, A., Conil, S., Cristofanelli, P., Cuevas, E., Daube, B., Davis, K., Mazière, M. D., Delmotte, M., Desai, A., DiGangi, J. P., Dlugokencky, E., Elkins, J. W., Emmenegger, L., Fischer, M. L., Gatti, L. V., Gehrlein, T., Gerbig, C., Gloor, E., Goto, D., Haszpra, L., Hatakka, J., Heimann, M., Heliasz, M., Hermanssen, O., Hintsa, E., Holst, J., Ivakhov, V., Jaffe, D., Joubert, W., Kang, H.-Y., Karion, A., Kazan, V., Keronen, P., Ko, M.-Y., Kominkova, K., Kort, E., Kozlova, E., Krummel, P., Kubistin, D., Labuschagne, C., Langenfelds, R., Laurent, O., Laurila, T., Lauvaux, T., Lee, J., Lee, H., Lee, C.-H., Lehner, I., Leppert, R., Leuenberger, M., Lindauer, M., Loh, Z., Lopez, M., Machida, T., Mammarella, I., Manca, G., Marek, M. V., Martin, M. Y., Matsueda, H., McKain, K., Miles, N., Miller, C. E., Miller, J.B.,Moore,F., Morimoto,S.,Munro,D.,Myhre, C.L.,Mölder,M.,Müller-Williams, J.,Nichol,S.,Niwa,Y.,OD oherty,S., Obersteiner, F., Piacentino, S., Pichon, J. M., Pittman, J., Plass-Duelmer, C., Ramonet, M., Richardson, S., Rivas, P. P., Saito, K., Santoni, G., Sasakawa, M., Scheeren, B., Schuck, T., Schumacher, M., Seifert, T., Sha, M. K., Shepson, P., Sloop, C. D., Smith, P., Steinbacher, M., Stephens, B., Sweeney, C., Timas, H., Torn, M., Trisolino, P., Turnbull, J., Tørseth, K., Viner, B., Vitkova, G., Watson, A., Wofsy, S., Worsey, J., Worthy, D., Zahn, A., and di Sarra, A. G.: Multi-laboratory compilation of atmospheric methane data for the period 1983-2020; obspac_ch4_1_GLOBALVIEWplus_v4.0_2021-10-14, `https://doi.org/10.25925/20211001`, 2021.

Segers, A., Steinke, T., and Houweling, S.: Description of the CH4 Inversion Production Chain, CAMS (Copernicus Atmospheric Monitoring Service) Report.. [online] Available from: `https://atmosphere.copernicus.eu/sites/default/files/2022-10/CAMS255_2021SC1_D55.5.2.1-2021CH4_202206_production_chain_CH4_v1.pdf` (Accessed 1 february), 2022.

Tarantola, A.: Inverse problem theory, Elsevier, Amsterdam, the Netherlands, 1987.

Tian, H., Lu, C., Ciais, P., Michalak, A. M., Canadell, J. G., Saikawa, E., Huntzinger, D. N., Gurney, K. R., Sitch, S., Zhang, B., Yang, J., Bousquet, P., Bruhwiler, L., Chen, G., Dlugokencky, E., Friedlingstein, P., Melillo, J., Pan,

S., Poulter, B., Prinn, R., Saunois, M., Schwalm, C. R. and Wofsy, S. C.: The terrestrial biosphere as a net source of greenhouse gases to the atmosphere, Nature, 531(7593), 225–228, doi:10.1038/nature16946, 2016.

Thanwerdas, J., Saunois, M., Pison, I., Hauglustaine, D., Berchet, A., Baier, B., Sweeney, C., and Bousquet, P.: How do Cl concentrations matter for the simulation of CH4 and 13C(CH4) and estimation of the CH4 budget through atmospheric inversions?, Atmos. Chem. Phys., 22, 15489–15508, https://doi.org/10.5194/acp-22-15489-2022, 2022.

Tsuruta, A., Aalto, T., Backman, L., Hakkarainen, J., Laan-Luijkx, I. T. van der, Krol, M. C., Spahni, R., Houweling, S., Laine, M., Dlugokencky, E., Gomez-Pelaez, A. J., Schoot, M. van der, Langenfelds, R., Ellul, R., Arduini, J., Apadula, F., Gerbig, C., Feist, D. G., Kivi, R., Yoshida, Y. and Peters, W.: Global methane emission estimates for 2000–2012 from CarbonTracker Europe-CH4 v1.0, Geosci. Model Dev., 10(3), 1261–1289, doi:10.5194/gmd-10-1261-2017, 2017.

Vogelezang, D. H. P. and Holtslag, A. A. M.: Evaluation and model impacts of alternative boundary-layer height formulations, Bound.-Lay. Meteorol., 81, 245–269, 1996.

Wang, F., Maksyutov, S., Tsuruta, A., Janardanan, R., Ito, A., Sasakawa, M., Machida, T., Morino, I., Yoshida, Y., Kaiser, J. W., Janssens-Maenhout, G., Dlugokencky, E. J., Mammarella, I., Lavric, J. V. and Matsunaga, T.: Methane Emission Estimates by the Global High-Resolution Inverse Model Using National Inventories, Remote Sens., 11(21), 2489, doi:10.3390/rs11212489, 2019a.

Watanabe S, Hajima T, Sudo K, Nagashima T, Takemura T, Okajima H, Nozawa T, Kawase H, Abe M, Yokohata T, Ise T, Sato H, Kato E, Takata K, Emori S, Kawamiya M: MIROC-ESM 2010: model description and basic results of CMIP5-20c3m experiments. Geosci Model Dev 4(4):845–872. https://doi.org/10.5194/gmd-4-845-2011, 2011

Weber, T., Wiseman, N. A., and Kock, A.: Global ocean methane emissions dominated by shallow coastal waters, Nat. Commun., 10, 1–10, https://doi.org/10.1038/s41467-019-12541-7, 2019.

Yoshida, Y., Kikuchi, N., Morino, I., Uchino, O., Oshchepkov, S., Bril, A., Saeki, T., Schutgens, N., Toon, G. C., Wunch, D., Roehl, C. M., Wennberg, P. O., Griffith, D. W. T., Deutscher, N. M., Warneke, T., Notholt, J., Robinson, J., Sherlock, V., Connor, B., Rettinger, M., Sussmann, R., Ahonen, P., Heikkinen, P., Kyrö, E., Mendonca, J., Strong, K., Hase, F., Dohe, S., and Yokota, T.: Improvement of the retrieval algorithm for GOSAT SWIR XCO2 and XCH4 and their validation using TCCON data, Atmos. Meas. Tech., 6, 1533–1547, https://doi.org/10.5194/amt-6-1533-2013, 2013.

Zheng, B., Chevallier, F., Ciais, P., Yin, Y. and Wang, Y.: On the Role of the Flaming to Smoldering Transition in the Seasonal Cycle of African Fire Emissions, Geophys. Res. Lett., 45(21), 11,998-12,007, doi:10.1029/2018GL079092, 2018a.

Zheng, B., Chevallier, F., Ciais, P., Yin, Y., Deeter, M. N., Worden, H. M., Wang, Y., Zhang, Q. and He, K.: Rapid decline in carbon monoxide emissions and export from East Asia between years 2005 and 2016, Environ. Res. Lett., 13(4), 044007, doi:10.1088/1748-9326/aab2b3, 2018b.